Formatted

APPENDIX IV

DETAILS OF CASK RESPONSE TO FIRE ACCIDENTS

Table of Contents

IV.1 Introduction 6
IV.2 CAFE Finite Volume Domain and Boundary Conditions 7
IV.3 The Rail-Steel Cask 9
IV.3.1 Geometric Consideration 10
IV.3.2 Rail-Steel Thermal Behavior and Model Assumptions 18
IV.3.3 Rail-Steel Materials and Thermal Properties 20
IV.3.4 Rail-Steel P-Thermal Finite Element Model and Boundary Conditions 28
IV.3.5 Rail-Steel Thermal Analysis Results 31
IV.4 Rail-Pb 31
IV.4.1 Geometry Considerations 42
IV.4.2 Rail-Pb Thermal Behavior and Model Assumptions 45
IV.4.3 Rail-Pb Materials and Thermal Properties 48
IV.4.4 Rail-Pb P-Thermal Finite Element Model 52
IV.4.5 Rail-Pb Thermal Analysis Results 52
IV.5 CAFE Benchmark 64

List of Figures

Figure IV-1. CAFE three-dimensional domain: (a) CAFE regulatory fire, (b) cask on ground and at the center of the pool, (c) cask on the ground and 3m (10ft)from the edge of the pool, (d) cask on the ground and 18.3m (60ft) from the edge of the pool. 9
Figure IV-2. Rail-Steel cask: (a) assembly of MPC and overpack, and (b) cask with limiters. 11
Figure IV-3. Rail-Steel overpack: (a) cross-sectional view through the center of the cask, (b) cross-sectional view through the mid-plane of the overpack 11
Figure IV-4. Rail-Steel MPC: (a) cross-sectional view through the axis of the cask, (b) cross-sectional through the midplane of the overpack. 13
Figure IV-5. Fuel assembly (a) and fuel rod (b). 15
Figure IV-6. Fuel-basket region (left) and equivalent fuel-basket region (right). 16
Figure IV-7. Rail-Steel upper (a) and lower (b) impact limiters. 17
Figure IV-8. Rail-Steel finite element mesh. 30
Figure IV-9. Rail-Steel Regulatory Uniform Heating Results (P-Thermal) 32
Figure IV-10. Rail-Steel CAFE regulatory fire. 34
Figure IV-11. Rail-Steel CAFE fire with cask on ground and at the pool center. 36
Figure IV-12. Rail-Steel CAFE fire with cask on ground 3.0m (10ft) from the edge of the pool. 38
Figure IV-13. Rail-Steel CAFE fire with cask on ground 18.3m (60ft) from the edge of the pool. 41
Figure IV-14. Rail-Pb components with the direct loaded fuel basket shown to the right. 43
Figure IV-15. Cross-section view of the Rail-Pb with the directly loaded fuel basket. 43
Figure IV-16. Axial burn up profile for the directly loaded fuel basket. 46
Figure IV-17. Three-dimension, quarter section of the directly loaded basket. The helium material is not shown. 47
Figure IV-18. The Rail-Pb mesh 53
Figure IV-19. Rail-Pb Regulatory Uniform Heating Results 54
Figure IV-20. Rail-Pb CAFE Regulatory Fire 56
Figure IV-21. Rail-Pb cask on ground at the pool center. 58
Figure IV-22. Rail-Pb cask on ground 3.0m (10ft) from the edge of the pool. 60
Figure IV-23. Rail-Pb cask on ground 18.3m (60ft) from the edge of the pool. 62
Figure IV-24. Large calorimeter fire test: (a) test setup and (b) fire fully engulfing the calorimeter. 65
Figure IV-25. Side view (looking from the north) of calorimeter and test setup. Note: the calorimeter is centered with the pool. This drawing is not to scale. 65

Figure IV-26. CAFE benchmark results using fully engulfed large calorimeter: (a) temperatures average along the 0, 90, 180, and 270 degree side looking at the calorimeter from the negative z-direction, and (b) temperatures averaged over each ring starting from Ring 1 located on the positive side of the z-axis. 66
Figure IV-27. CAFE benchmark results using a small calorimeter 1.5m (4.9ft) from the edge of the fire. 67

List of Tables

Table IV-1. Axial burn up profile in the active fuel region. 18
Table IV-2. Thermal conductivities for the Rail-Steel materials. 22
Table IV-3. Specific heat for the Rail-Steel materials. 22
Table IV-4. Densities for the Rail-Steel materials. 23
Table IV-5. Emissivity for some of the Rail-Steel materials and paints. 23
Table IV-6. Effective thermal conductivity for the fuel-basket region. 25
Table IV-7. Effective thermal conductivity of the aluminum heat conduction elements. 26
Table IV-8. Effective thermal conductivity of the intermediate shells in the in-plane directions. 27
Table IV-9. Effective conductivity of the neutron shield region. 28
Table IV-10. Thermal conductivities for the Rail-Pb materials. 49
Table IV-11. Specific heat for the Rail-Pb materials. 49
Table IV-12. Densities for the Rail-Pb materials. 49
Table IV-13. Emissivity for some of the Rail-Pb materials. 50
Table IV-14. Effective thermal properties of the directly loaded fuel basket. 52
Table IV-15. Effective thermal conductivities for the neutron shield region of the Rail-Pb. 53

APPENDIX IV

DETAILS OF CASK RESPONSE TO FIRE ACCIDENTS

IV.1 Introduction

A thermal analysis of Rail-Steel and Rail-Pb package types is performed to obtain the thermal response of these casks. The approach used to model the Rail-Steel and the Rail-Pb is similar to the ones used in the HI-STAR 100 and NAC-STC Safety Analysis Reports (SARs) (Holtec International, 2004, Nuclear Assurance Corporation International, 2004), a combination of thermal resistor network analysis and finite element modeling. The thermal resistor network method is used to obtain effective thermal properties for several regions of the casks. These homogenized regions are then added to the finite element model with equivalent effective properties. This process eliminated some of the geometric redundancies and/or discretization complexities inherent in the models, while at the same time keeping the essential thermal response of the packages.

For the Rail-Steel, assumptions and results reported in the Rail-Steel SAR (Holtec International, 2004) are used, but modified where necessary to reflect the current study. The approach used to model the Rail-Pb is similar to the approach used in the Rail-Pb SAR (Nuclear Assurance Corporation International, 2004). The only exception is in how the contents of the package are modeled. In the Rail-Pb SAR, the fuel-basket region and the rest of the overpack are modeled explicitly using a three-dimensional, quarter-section of the cask to obtain a steady-state solution. The maximum temperature difference between the center of the fuel-basket region and the inner wall of the overpack obtained in the steady-state solution is then used to calculate the fuel-basket cladding temperature for the regulatory uniform heating flux (see 10CFR71.73), which did not include a fuel-basket region. Here, a quarter section of the fuel basket is used to obtain effective thermal properties for the basket. The fuel-basket region is replaced in the full-scale, finite element model using effective properties for the homogenized basket region. As in the Rail-Steel analysis, assumptions and results in the Rail-Pb SAR are used to obtain the thermal response of this cask; again, with minor changes to reflect the current study. Values taken from the Rail-Steel and the Rail-Pb SARs are checked where possible—using formulas taken directly from these reports or derived from independent analysis—to assess the validity of assumptions and to verify results; no significant deviations were found.

In general, boundary conditions and material properties are slightly different from those used in the Rail-Steel and Rail-Pb SARs. The intent of this thermal analysis is to determine the temperature of critical components during and after a hypothetical fire accident using material

Deleted: cask

Comment [csb1]: Two spaces after a sentence, this needs to be adjusted throughout the document.

Comment [csb2]: Be sure that any and all information from the SARs cited are from the publically available versions of the SARs, since this will be a public document.

Deleted: Acceptance

Comment [csb3]: I think you know that this should be modified throughout the document.

Deleted: casks

Deleted: Acceptance

Deleted: cask

Deleted: errors

Deleted: are

properties and boundary conditions that closely resemble the conditions in a real fire accident. Since realistic boundary conditions are sometimes difficult to implement using available data and/or current analysis tools, some simplifications had to be made. For example, NS-4-FR, the insulation material used in the neutron shields of both packages, is assumed to decompose completely when its operational temperature limit is reached. In such cases, conservative assumptions are made to maximize heat input to the packages, as is done in both SARs cited above. In the case of material properties, those presented in the SARs are preferred, followed by those in standard thermal textbooks and journals. For some materials, like NS-4-FR, properties are available but only over a limited temperature range. In such cases, the value available at the highest temperature is used throughout the rest of the temperature range.

Comment [csb4]: Does this have a copyright/trademark or other pointer that should be brought out?

Comment [csb5]: Is it clear that Holtite A is NS4FR

Deleted: the both cask

Deleted: casks

As mentioned in Chapter 4, MSC PATRAN-Thermal (P-Thermal) (MSC, 2008) is the finite element heat transfer code used to solve the internal thermal response of the Rail-Steel and Rail-Pb in the regulatory uniform heating scenario. This scenario effectively simulates fire conditions using a spatially uniform radiation flux over the external surfaces of the casks as established in 10 CFR 71.73. CAFE (Container Analysis Fire Environment) is the computational fluid dynamics (CFD) code used to generate the fire environment for the CAFE regulatory and CAFE non-regulatory scenarios described in Chapter 4. For these scenarios, CAFE and P-Thermal are coupled together to obtain the thermal response of the Rail-Steel and Rail-Pb casks. CAFE generates more realistic fire conditions on the external surfaces of the casks, as opposed to spatially uniform heating conditions. P-Thermal uses CAFE-predicted, external conditions to calculate the internal thermal response of the casks.

Comment [csb6]: These paragraphs are at 1.15 line spacing. I believe that all of the document should be at 1.0 line spacing. It alternates between 1.15 and 1.0 throughout this document.

In the following sections, the geometry, material properties, and boundary conditions used to model the Rail-Steel and the Rail-Pb packages are described, and results that supplement discussions in Chapter 4 are shown. The three-dimensional domain and the boundary conditions used in the CAFE runs are described first, followed by the geometry and boundary conditions used in the Rail-Steel and Rail-Pb P-thermal finite element models. Finally, results from two CAFE benchmark runs are presented.

IV.2 CAFE Finite Volume Domain and Boundary Conditions

CAFE (Suo-Antilla et al., 2005) uses the finite volume approach with orthogonal Cartesian discretization to solve: (1) the three momentum equations for predicting the velocity and momentum field, (2) the mass continuity equation, (3) the energy equation for predicting the temperature field, (4) the equation of state, (5) a number of scalar transport equations for tracking the flow of species, and (2) two transport equations to solve thermal radiation within and external to the fire. CAFE uses a variable density PISO algorithm to obtain a velocity field which satisfies both the momentum and continuity equations. CAFE has a number of turbulence models, but for this study a large eddy simulation formulation is used. Thermal radiation transport within and near the fires is split into two types: diffusive radiation inside the flame zone and clear air radiation outside the flame zone. Diffusive thermal radiation transport is modeled

Comment [csb7]: Acronym?

Deleted: outside

with the Rosseland approximation. Clear air radiation outside the flame zone is modeled using view factor methods.

CAFE is coupled to P-Thermal through a set of user subroutines that are responsible for passing temperature and thermal heat flux data between both codes. CAFE uses a specialized scheme to map the temperature and heat fluxes to the exterior surfaces of the finite element model (Suo-Antilla et al., 2005). MSC PATRAN is the front end code employed to generate the material database, the finite element discretization, and the boundary conditions used by P-Thermal. It is through a special boundary condition, setup in PATRAN, that CAFE and P-Thermal are able to exchange data.

Figure IV-1 illustrates the domain configurations used in the CAFE fire scenarios discussed in Chapter 4. Figure IV-1(a) shows the computational fluid dynamics domain used for the CAFE regulatory run, and Figures IV-1b through IV-1d show the domain for the CAFE non-regulatory runs. As explained in Chapter 4, all non-regulatory CAFE runs were determined based on the severity and frequency of occurrence of the scenario. A square pool is used to assure the specifications from 10CFR71.73 are met in the case of regulatory fires. For consistency the pool remained a square in all other cases. The pool area is 9.25x13.80m (30.35x45.28ft) in the Rail-Steel configurations,

Deleted: likelihood

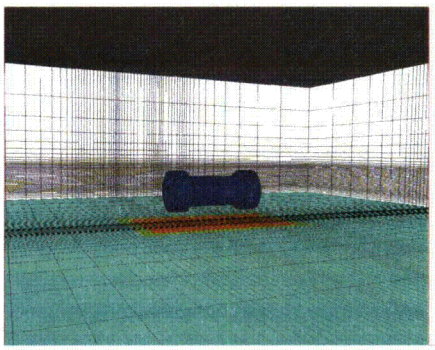

(a)

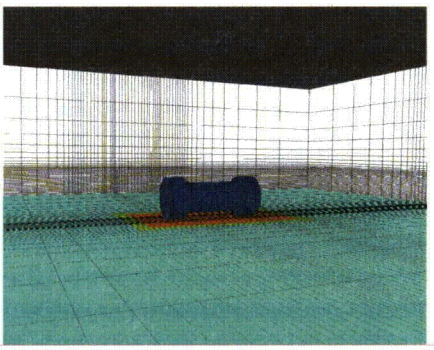

(b)

Comment [csb8]: These figures are a little fuzzy, may be fine when printed in a full size document.

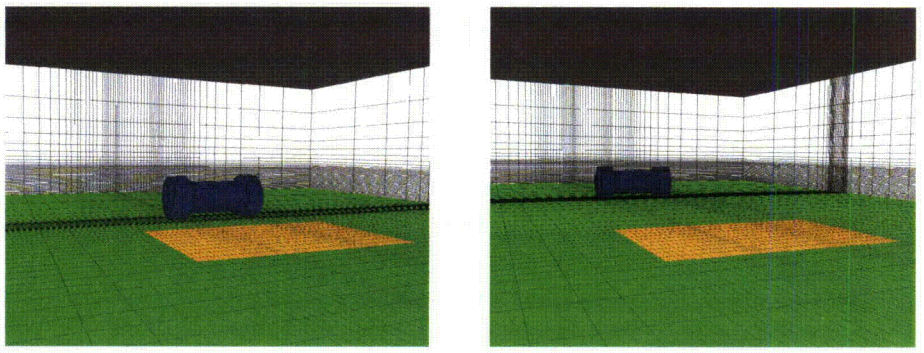

(c) (d)

Figure IV-1. CAFE three-dimensional domain: (a) CAFE regulatory fire, (b) cask on ground and at the center of the pool, (c) cask on the ground and 3m (10ft)from the edge of the pool, (d) cask on the ground and 18.3m (60ft) from the edge of the pool.

and 9.14x12.42m (29.99x40.75ft) in the Rail-Pb configurations. These pool areas corresponded to a fully-loaded rail tank car burning over a period of 3 hours, the maximum burn time based on 113.6m^3 (30,000 gallons) of fuel. The pool edges remained 3m (9.8ft) away from the surface of the package in all runs.

Deleted: casks

An appropriate domain size is determined from del Valle et. al. (2007) and from del Valle (2009), in which thermal analyses were conducted with CAFE using a calorimeter the size of a rail cask. In these studies, results of CAFE runs are compared to experiments and showed good agreement. In the current study, the ground dimensions varied between cases since a larger domain is required for the cask offset cases, but are at least 25x15x25m (82x49x82ft), about the size of the domain used in del Valle et. al. (2007) and del Valle (2009). A mesh refinement study is conducted to assess the sensitivity of the cask external temperatures to mesh size and to determine an appropriate mesh size. Approximately 145,000 finite volumes are used in this study for both casks. Slightly hotter temperatures are observed on the bottom of the cask (on the order of XXX°C [xxx°F]) when finer grids are used, but the differences are not sufficient to outweigh the extra computational expense. As observed in Figure IV-1, the mesh is finer in the region near the pool. All CAFE scenarios used calm wind conditions; the velocity at the boundaries and inside the domain are originally set to zero, but are allowed to float as the fire develops.

Deleted: both

IV.3 The Rail-Steel Cask

The Rail-Steel packge, is designed for transportation of a variety of nuclear spent fuel assemblies and is intended to fit horizontally in a rail car bed. Therefore, the Rail-Steel system is assumed to be in the horizontal position in all CAFE runs (see Figure IV-1), as it would be after derailment if the flatbed rail car overturns or if the cask is ejected from a rail car. Only the thermally relevant components of the Rail-Steel are considered in this thermal analysis. As stated in the

Deleted: cask

Deleted: is a packaging system

Comment [csb9]: May need to discuss a specially designed rail car here…this is not just strapped to any flat rail car bed.

Deleted: cask

introduction, some results reported in the Rail-Steel SAR (Holtec International, 2004) are used in this analysis. Values taken from this report are checked where possible to assess validity of assumptions and to verify results.

IV.3.1 Geometric Consideration

The Rail-Steel cask consists of an overpack, a multipurpose canister (MPC), and two impact limiters; these components fit together as shown in Figure IV-2. The MPC stores the nuclear spent fuel material, and is sealed tight to prevent the contents from leaking into the overpack inner cavity. The MPC is the first containment barrier in the Rail-Steel cask. The overpack is designed to attenuate both the heat, and the neutron and gamma rays generated inside the MPC. The overpack is also sealed tight to prevent the contents from a breached canister from further leaking into the external environment; thus, the overpack forms the second containment barrier in the Rail-Steel. During transportation, the overpack ends are fitted with impact limiters that, besides absorbing most of the impact energy during an impact, add an additional thermal insulation layer to the extreme ends of the overpack when intact.

IV.3.1.1 The Overpack

The Rail-Steel overpack is a multilayered cylindrical vessel approximately 2.11m (83.3in) in diameter and 5.16m (203.1in) in length. The inner cavity of the overpack is approximately 1.75m (64.7in) in diameter and 4.85m (191.1in) in length. The inner cavity is formed by (1) welding a thick wall cylinder, called the inner shell, to a metal base cup at the bottom and to a large diameter vacuum flange at the top, and (2) bolting a closure plate onto the flange as shown in Figure IV-3. Five thin wall cylinders, tightly fitted to one another and to the inner shell, form the next structural layer of the overpack, strengthening the overpack against puncture or penetration. These cylinders are jointly referred to as the intermediate shells and act as the gamma shield. Channels welded to the outermost intermediate shell extend radially outward and delimit the last layer of the overpack. These channels act as fins enhancing conduction to the periphery of the overpack. Plates welded between the ends of each successive channel complete the outer enclosure shell of the overpack. The cavities formed between the channel walls, and between the outermost intermediate shell and the outer enclosure plates are filled with a neutron shield material which provides thermal insulation in addition to neutron attenuation. The outermost intermediate shell, the neutron shield region, and the outer enclosure shell effectively extend the diameter of the overpack an additional 32.3cm (12.7in) beyond the perimeter of the flange and the metal base cup.

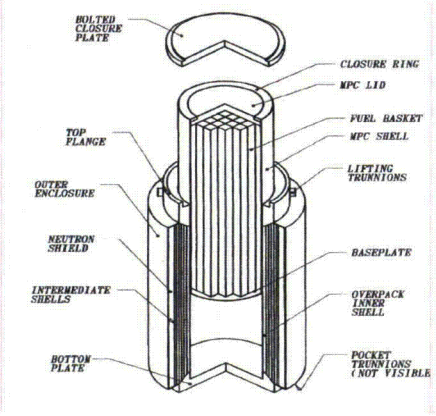

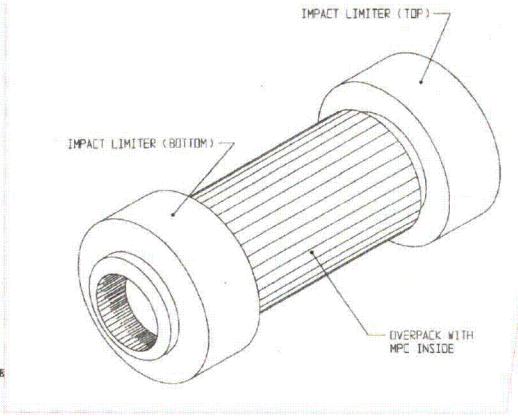

(a) (b)

Figure IV-2. Rail-Steel cask: (a) assembly of MPC and overpack, and (b) cask with limiters.

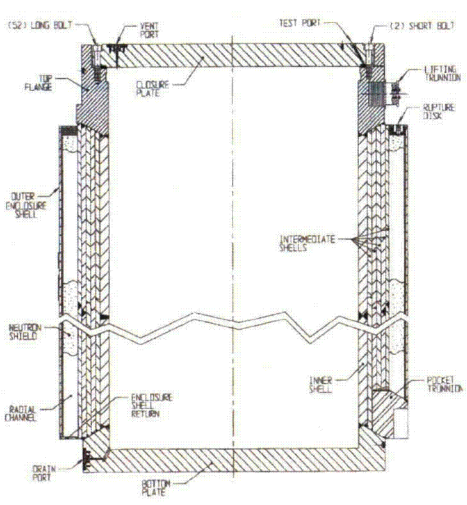

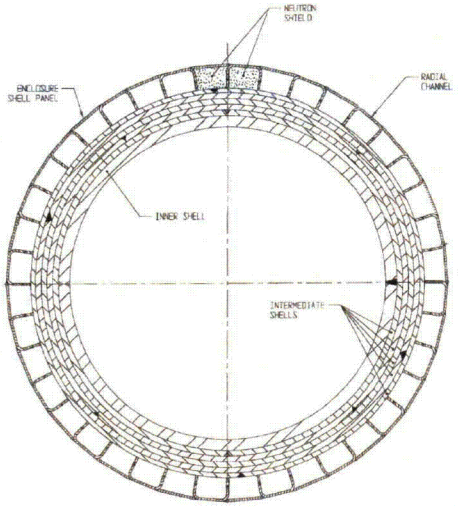

(a) (b)

Figure IV-3. Rail-Steel overpack: (a) cross-sectional view through the center of the cask, (b) cross-sectional view through the mid-plane of the overpack.

Comment [csb10]: Be sure to reference all the figures that come from the HOLTEC SAR

The overpack shells, metal base cup, vacuum flange, closure plate, and neutron shield region are the major components of the overpack and together comprise most of its volume. The overpack shells, metal base cup, vacuum flange, and closure plate are represented explicitly in the thermal model with minor alterations to simplify the solid modeling and meshing process. The most significant change is extending the length of the overpack shells through the length of the neutron shell region. Note these length changes are expected to have a minor effect on the overall thermal response of the overpack, and only in the radial direction. The intermediate shells and the neutron shield region are each represented as a single volume also to minimize geometric complexity; however, their thermal properties are properly accounted for in the thermal model using the techniques described in Sections IV.3.3.3 and IV.3.3.4.

Comment [csb11]: Not clear on exactly what is being done here…is this general practice, do you have any sensitivity information about this?

Comment [csb12]: When I print this out it says that there is an error and that there is not a reference source found…I assume this will not be a problem in the final document.

The overpack contains additional components used to service the overpack during normal operations or designed to function only during abnormal ambient conditions such as fires. These features include seals, gas ports, rupture disks, and lifting and pocket trunnions as observed in Figure IV-3. These components are not included in the model because their effects are assumed: (1) negligible due to their small volume and mass relative to the other components in the overpack, (2) highly localized with no effect to the overall thermal performance of the package at locations of interest, or (3) both.

IV.3.1.2 Multipurpose Canister

The MPC is a cylindrical vessel approximately 1.73m (68.3in) in diameter (outside) and 4.83m (190.3in) in length. The MPC is made from a cylindrical shell 1.2cm (0.5in) thick and 4.76m (187.4in) in length, a circular baseplate 6.35cm (2.5in) thick, and a circular plate lid 24.1cm (9.5in) thick (see Figure IV-4a). The baseplate is welded to the bottom of the MPC shell, and this shell is intern welded to the exterior surface of the lid. At the top, the MPC shell is flushed against a large groove on the end perimeter of the circular plate lid. An annular closure ring welded on the groove and to the top of the shell seals the contents of the MPC. In the horizontal position, the shell and the base plate rest on the inner shell of the overpack. Drain and vent ports on the MPC lid are used to evacuate and fill the MPC with a inert gas (generally helium). With the exception of the closure ring and drain ports, all these components are modeled explicitly. The closure ring is assumed to be part of the lid.

Deleted: ed

Deleted: known

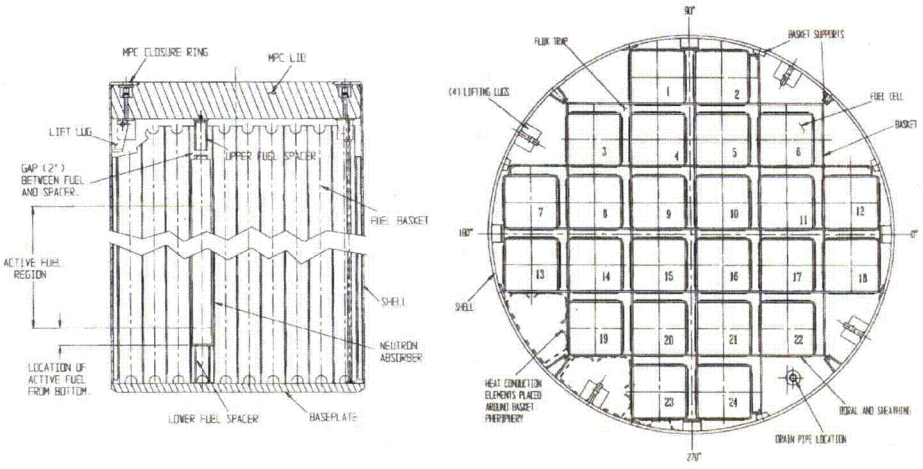

(a) (b)

Figure IV-4. Rail-Steel MPC: (a) cross-sectional view through the axis of the cask, (b) cross-sectional through the midplane of the overpack.

The SNF (or SNF assemblies) is stored in a fuel basket inside the MPC (see Figure IV-4b). The fuel basket is made by welding a series of perpendicular and parallel plates to form an array of storage cells. Each storage cell contains a single fuel assembly. The MPC is designed to carry two types of fuel baskets: (1) the MPC-24, which contains a maximum of 24 PWR fuel assemblies; and (2) the MPC-68, which contains a maximum of 68 BWR assemblies. Both fuel baskets are similar in design; however, the MPC-24 is designed to carry a greater heat load. For this reason, attention is focused on the MPC-24. In the MPC-24, the fuel cells are physically separated from one another by a gas pocket called the flux trap. The length of the fuel basket is approximately 4.48m (176.5in). The fuel assembly may not exceed this length; in such cases, spacers are installed on the baseplate and on the MPC lid to hold the fuel assemblies in place (see Figure IV-4a).

A single fuel assembly consists of an array of fuel rods, each rod separated by a gas space (in the package when backfilled) as shown in Figure IV-5a. The total number of rods per assembly varies with fuel assembly design. Each fuel rod however consists of a number of cylindrical fuel pellets fitted into a thin walled pipe, called the fuel cladding. The fuel cladding, inner diameter is slightly larger than the diameter of the pellets as shown in Figure IV-5b. The fuel pellets are held tightly against each other using the force of a spring. The radial dimensions of the rod components vary between fuel rod designs. In general, the length of the fuel column is only a fraction of the total length of the fuel rod and marks the active fuel region. The total length of the

Deleted: nuclear spent fuel material

Comment [csb13]: What about the MPC 32, any particular reason the MPC 24 was chosen?

Deleted: extend

fuel rod is approximately the same as the length of the fuel assembly. Additional supports are added to the ends of the fuel assembly and at regular intervals along the length of the assembly for structural integrity, to maintain spacing between the rods, and for handling purposes.

The Rail-Steel system is designed to carry a number of PWR fuel rods; it's impractical to analyze the Rail-Steel system with all these fuel rod designs. Similarly, it's impractical to model the MPC contents with all the components described above because: (1) the wide range of component length scales creates additional meshing complexities, and (2) alternative methods have been employed in the SAR literature and in this study to obtain equivalent thermal properties for the MPC internal contents with good results (see Section IV.4.4). Hence, the fuel-basket region, which includes the fuel assembly, basket walls, and flux trap gaps, is not represented explicitly in the Rail-Steel model.

The MPC shell contains support structures that help keep the fuel basket laterally in place and lift logs which are used during loading and unloading operations. Some slots between the periphery of the fuel basket and the MPC shell wall contain thin wall heat conduction elements. These conduction elements extend the full length of the basket and provide an effective heat conduction path between the MPC basket and MPC shell. With the exception of the heat conduction elements, all other structural elements in the fuel-basket periphery region are ignored for the same reason cited in Section IV.3.1.1. The fuel heat conduction elements are not represented explicitly, but their thermal effect is included through the use of a simplified analytical model explained in the Rail-Steel SAR.

To simplify the modeled geometry, the fuel-basket region and fuel-basket periphery region are modeled as two concentric cylindrical regions extending the length of the fuel assembly (see Figure IV-6). The diameter of the equivalent fuel-basket region (Zone 1) is calculated in Holtec International (1997) using the hydraulic diameter of the fuel-basket periphery region

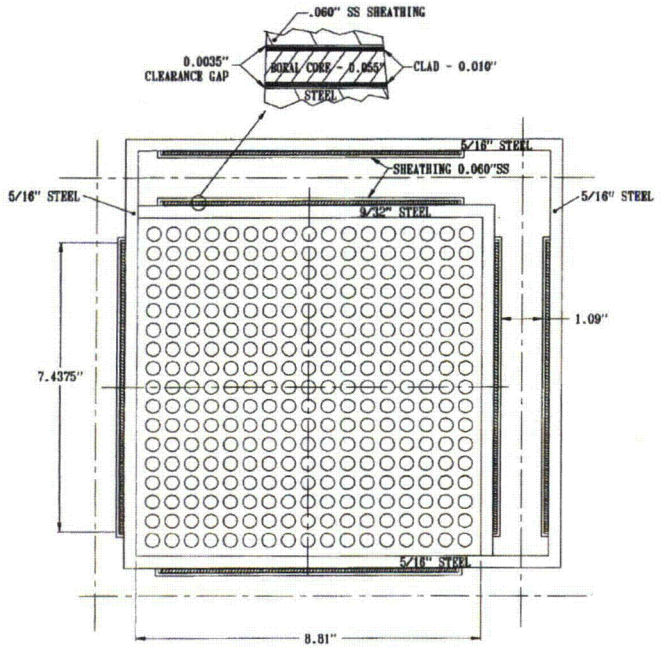

(a)

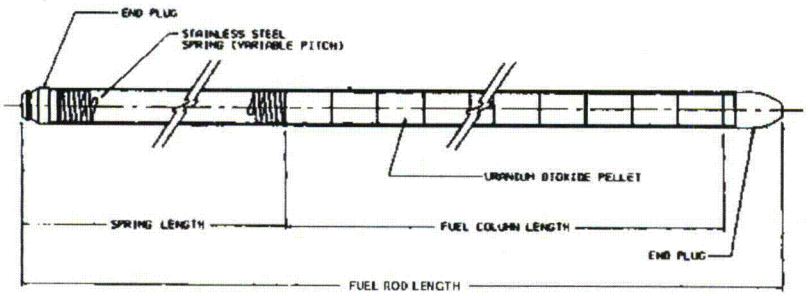

(b)

Figure IV-5. Fuel assembly (a) and fuel rod (b).

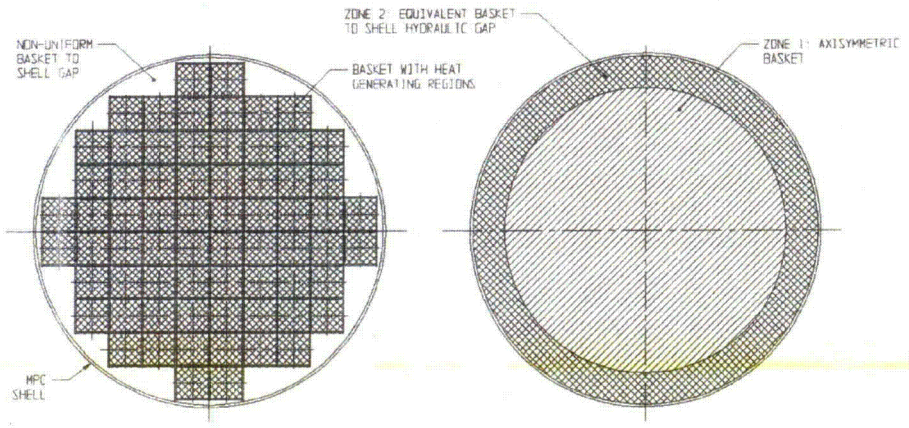

Figure IV-6. Fuel-basket region (left) and equivalent fuel-basket region (right).

(Zone 2). The hydraulic diameter takes into account the perimeter of the fuel basket and MPC inner shell wall, and the average basket-to-shell gap length—indirectly obtained from total surface area between the perimeter of the fuel basket and MPC inner wall—through which heat transfer occurs. For the MPC-24 basket, the hydraulic diameter is approximately 12.7cm (5in) (Holtec International, 1997). The hydraulic diameter is also equal to the inner diameter of the MPC shell minus the inner diameter of the equivalent fuel-basket cylinder region; in this way the equivalent fuel-basket cylinder diameter and periphery annulus gap length may be obtained.

IV.3.1.3 Rail-Steel Impact Limiters

The impact limiters are relatively low density cylindrical components that are not only designed to absorb energy during impact but also serve as insulators during fires in the uncrushed state. The main body of the impact limiter has a maximum diameter of 3.25m (128in) and a maximum length of 1.52m (60in) Figure IV-6.

Most of the impact limiter is honeycomb material enclosed in a thin shell metal wall. The honeycomb material and outer shell walls are supported in the interior of the limiter by a large-diameter circular plate welded (1) on one side to a small-diameter, thin-wall, cylinder and (2) on the perimeter to a large-diameter, thick wall, cylinder. The small- and large-diameter cylinders extend axially outward from the large-diameter plate into the interior of the limiter a distance of approximately 54.9cm (21.6in) and 34.6cm (13.5in), respectively. The small diameter cylinder

forms the smallest diameter cavity in the impact limiter, on the side facing the external environment. This air-filled cavity is covered with a circular plate. In the upper limiter, the large

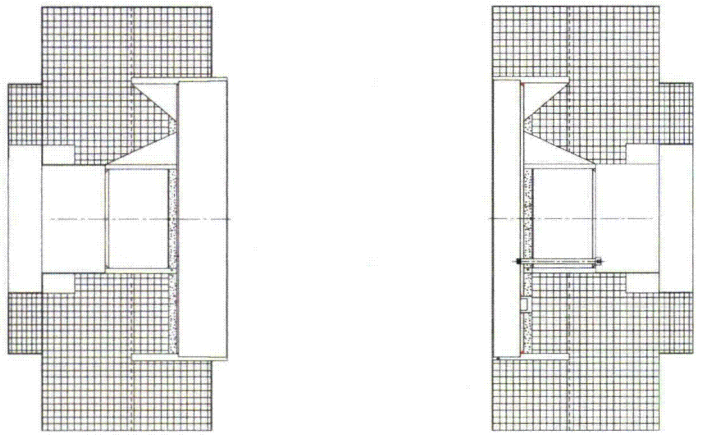

(a) (b)

Figure IV-7. Rail-Steel upper (a) and lower (b) impact limiters.

diameter cylinder also extends in the opposite direction a distance of 36.8cm (14.5in) from the large-diameter plate, protruding beyond the surface of the limiter facing the overpack. In the lower limiter, the large-diameter cylinder only extends from the large-diameter plate to the surface of the limiter. Triangular channels are welded to the large-diameter plate and to the large- and small-diameter cylinders at regular angular intervals in the interior of the impact limiter. Each impact limiter contains a circular segment of neutron shielding, 6.35m (2.5in) thick, next to the large-diameter plate and between the triangular channels. This neutron shield provides axial neutron attenuation and serves as a heat barrier between the impact limiter body and the overpack ends. The neutron shield is covered at the other end by a thin shell wall.

The overpack fits into the cavity formed by the large diameter cylinder and the large diameter plate. The top upper limiter bolts into the sides of the vacuum flange through the protruding ends of the large diameter cylinder. The lower limiter is secured into the metal base cup using bolts that extend from the circular plate to just past inner surface of the large diameter plate as shown in Figure IV-7b.

Comment [csb14]: This is a little difficult to follow.

The (impact?) limiters are assumed to stay intact after the hypothetical accident scenarios described in Chapter 4. This assumption is reasonable since the height of the flatbed rail car is approximately that of the diameter of the overpack. This height precludes any significant damage to the impact limiter during an accident scenario involving, for example, the overturn of the rail

Deleted: overpack

car flatbed, or the Rail-Steel package falling off the flatbed. Since the limiters are assumed to stay intact, they are modeled in their original shape. The impact limiter, shell walls are not considered. The neutron shield material in the limiters is retained since it serves as a heat barrier between the main body of the limiter and the overpack. Only the large-diameter, thick-wall, cylinder is explicitly modeled since it serves as a direct conduction path from the exterior to the interior of the limiter.

Comment [csb15]: Unlikely given the type of tie downs for this package.

IV.3.2 Rail-Steel Thermal Behavior and Model Assumptions

The MPC-24 is designed to carry a maximum heat load of 20kW (0.833kW per fuel assembly). This heat generation rate is non-uniform along the length of the active fuel region. Table IV-1 shows the normalized, axial heat generation rate distribution for a typical Rail-Steel, PWR assembly (Holtec International, 2004). This table is used in Holtec International (1997) to calculate the heat generation rate through the active length of the basket (i.e., in the axial direction). The Rail-Steel system is designed to reject heat passively to the environment under normal conditions of transport. Thus, heat is dissipated from the fuel rods to the exterior surfaces of the cask only by a combination of conduction, convection, and radiation heat transfer modes.

Table IV-1. Axial burn up profile in the active fuel region.

Axial Distance from Bottom of Active Fuel(% of Active Fuel Length)	Normalized Value
0% to 4-1/6%	0.548
4-1/6% to 8-1/3%	0.847
8-1/3% to 16-2/3%	1.077
16-2/3% to 33-1/3%	1.105
33-1/3% to 50%	1.098
50% to 66-2/3%	1.079
66-2/3% to 83-1/3%	1.050
83-1/3% to 91-2/3%	0.960
91-2/3% to 95-5/6%	0.734
95-5/6% to 100%	0.467

Formatted: Font: Bold
Formatted: Space After: 0 pt
Formatted Table
Formatted: Space After: 0 pt, Line spacing: single
Deleted: ¶

For normal transportation conditions, the external temperature is higher than the internal temperature of the cask; therefore, heat will be dissipated outwardly starting from the fuel rods. Inside the fuel rods, heat is dissipated outward by (1) conduction through the gas space between rods; and (2) by radiation exchange between the fuel rods, and between the fuel rods and the walls of the basket. Convection is assumed negligible in this region since radiation effects dominate at high temperatures. Heat is then dissipated by conduction through the gas space in the flux traps, and by radiation between the basket walls. Convection is also assumed negligible in flux trap region. In the fuel-basket periphery, heat is dissipated to the MPC shell (1) by conduction through the heat conduction elements and the gas; and (2) by radiation between the

Deleted:

walls of the fuel basket and the MPC, and between the inner walls of the heat conduction elements. In this region, convection enhances heat transfer between the inner walls of the heat conduction elements through the Rayleigh effect; this effect is taken into account through the results provided in the Rail-Steel SAR. There a two-dimensional, finite element model is used to determine the heat convection coefficient for this region of the basket.

Heat transfer from the MPC shell to the overpack inner shell occurs through a MPC-overpack non-concentric gap. In the horizontal position the MPC makes contact with the overpack at the bottom. This contact gap is approximately 0.5 mm (0.02in) across. In this region, heat is also dissipated by conduction through the variable gas-filled gap, and by radiation between the outer and inner walls of the MPC and overpack, respectively. A two-dimensional, analytical model is used in the Rail-Steel SAR to obtain an effective conductivity through the variable length gap and is discussed in Section IV.3.3.2. Heat transfer through the inner and intermediate shells occurs by conduction through the shell material and through the contact gaps between the shells. These contact gaps are assumed to be five microns (2000 μ-in) across as in the Rail-Steel SAR. Conduction in the neutron shield region occurs in parallel through the radial connectors and the neutron shield material. A simple thermal resistor network is used to calculate the effective thermal conductivity through intermediate shells and through neutron shield region (see Sections IV.3.3.3 and IV.3.3.4).

The Rail-Steel tranportation system is designed to maintain the temperature of components below their operational temperature limits[1] for normal conditions of transport, and for a 30-minute, fully-engulfing, regulatory fire and subsequent cool down period (10CFR71.73). For longer fully-engulfing fires, such as the ones depicted in this study, a significant amount of heat may be transferred to the interior of the Rail-Steel cask, raising the temperature of some of its components above their operational temperature limits. This is expected to occur in the neutron shield region. The operational temperature limit of the neutron shield insulation is 149°C (300°F). In our model, the neutron shield material is assumed to decompose completely shortly after it reaches this temperature limit, immediately triggering thermal radiation exchange between the overpack enclosure shell and the outermost intermediate shell. The assumption used here is a significant departure from what is assumed in the SAR, but is conservative in that heat from the fire is transferred more efficiently to the interior layers of the overpack. More will be said in Section IV.3.3 regarding this topic. As with the neutron shield, the aluminum honeycomb is expected to reach temperatures beyond the operational temperature limits. However, the honeycomb material is not expected to completely melt. Given the results in Pierce et. al. (2003), the regression rate of the honeycomb material is expected to be minimal over a three hour period and have only a local effect.

Deleted: cask

Deleted: -period,

[1] The term operational temperature limit does not necessarily mean melting point. Operational temperature limits are given in the Rail-Steel SAR.

Heat dissipation through the cross section (i.e., in the axial direction) of the MPC and overpack, and through the limiters is assumed to occur mostly by conduction. Heat conduction occurs in parallel through each of the materials that comprise this cross section. Thermal radiation in the axial direction is possible; however, since view factors tend to diminish with the distance square and angle of view, and the temperature gradients are weak along the axis compared to on the in-plane, as observed in contour results presented in Chapter 4, these effects are neglected in the basket region. Thus, radiation effects are assumed to be mostly in the radial direction except near the lateral ends of the MPC. Thermal radiation exchange occurs between the MPC outer surface and the overpack inner lid and between the MPC outer surface and the overpack bottom plate. In the limiters, the thin metal shell covering the neutron shield radiates to the small diameter plate located directly across the air-gap that fills the small diameter cylinder (see Figure IV-7 and the description in Section IV.3.1.3).

With the exception of the contact gaps already mentioned (e.g., between intermediate shell layers and between MPC and overpack), all contact gaps in the Rail-Steel cask are assumed perfect. This assumption is conservative in that heat is allowed to penetrate the Rail-Steel cask with reduced thermal resistance.

IV.3.3 Rail-Steel Materials and Thermal Properties

The Rail-Steel system is made from a variety of steel and aluminum alloys. The overpack inner shell is made from SA203-E cryogenic steel, and the metal base cup, vacuum flange, and closure plate are made from SA350-LF3 cryogenic steel. The intermediate shells are made from SA516-70 carbon steel, and the radial channels and enclosure plates from SA515-70 carbon steel. The neutron shield material is Holtite-A, a synthetic neutron-absorbing polymer with one percent boron carbide sold commercially under the trade name NS-4-FR (Holtec International, 2004). The variable-length gap between the MPC and overpack is filled with helium.

The MPC shell, lid, and baseplate, and the basket, fuel-cell walls are made from alloy X, a generic term used in various SARs that usually stands for one of the following stainless steel metals: SA304, SA304LN, SA316, or SA316LN (Hotec International, 2004). The thermal properties of SA304 are assumed for these components. Very little difference in thermal properties is found between SA304 and the other stainless steel materials already mentioned. On one side of each fuel cell wall is a thin layer of Boral sandwiched between the fuel cell wall and thin stainless steel sheathing. Boral is a neutron absorber made of boron carbide and aluminum alloy 1100 (Holtec International, 2004). The Boral layer and stainless steel sheathing extend the length of the active fuel region. The MPC-24 is designed to carry intact zircaloy and stainless steel clad fuel assemblies. In this study, the fuel rods are assumed to be made from zircaloy cladding as done in the Rail-Steel cask for conservative results. The fuel pellets are uranium dioxide (UO_2). The MPC heat conduction elements are made from aluminum alloy 1100. All void spaces inside the MPC are filled with helium (Holtec International, 2004).

Deleted:

Deleted: 0

The honeycomb in the impact limiter is made from aluminum 5052, and the large-diameter, cylinder from carbon steel (SA516). The neutron shield segments are also made from Holtite-A.

Table IV-2 provides the thermal conductivity for materials used in the Rail-Steel at several temperatures. For aluminum 1100 and the various carbon steels, data from Rail-Steel SAR is available only over a limited temperature range since the analysis in that report showed cask temperatures within a limited range due to the limited 30 minute fire exposure and subsequent cool down. For these materials, the data trend is decreasing; therefore, the thermal conductivity value at the highest temperature is used at higher temperatures, a conservative assumption since the thermal conductivity values used are higher than what they should be. Note also that Holtite-A is replaced with air once the temperature of the neutron shield region reached the operational temperature limit of that material. In reality, only a fraction of the Holtite-A decomposes. Some of the gases generated in the shield region outgas through the neutron shield rupture disks at high pressures. Up to 90% of these gases come from moisture in the Holtite-A (Federal Register, 2000). Experiments show that up to fifty percent (by weight) of the NS-4-FR eventually degrades by the time temperature of the material reaches 800°C, leaving behind charred remains (Soo-Haeng et. al., 1996), and these are not expected to combust (Suo-Haeng et. al., 1996; Federal Register, 2000). The thermal conductivity of helium varies with pressure in addition to temperature; however, the pressure dependency is much weaker over the range of 101 to 689kPa (14 to 100lb/in^2) (Petersen, 1970).

Table IV-3 provides the specific heat for these same materials at several temperatures. Temperature dependent values are given only for those materials which exhibited large variation in temperature. With the exception of stainless steel, aluminum 5052, and carbon steel, the specific heat of most materials used in the Rail-Steel is fairly constant. Note, however, that limited data is available for Holtite-A. The specific heat of Holtite-A is assumed remain constant from 92°C to its operational temperature limit. Recall that air properties are used beyond this limit. The specific heat of carbon steel increases significantly over the stated range. Most of the change is slow at low temperatures, but then is sudden between 450 and 727°C (842 and 1340°F) (Incropera and Dewitt, 1996, Yafei, 2009) and reaches a peak at around 1010°C (1850°F), the Curie temperature. The specific heat quickly drops after reaching the Curie temperature. This behavior is associated with changes in the magnetic state of these materials and has been observed for a great number of carbon steel materials with various carbon contents (Yafei, 2009).

Comment [csb17]: Confusing…

Table IV-4 provides densities for stainless steel, carbon steel, zircaloy, and UO_2 at 92°C (200°F), and for air and helium at various temperatures. Since the density of most metals changes very little with temperature, only the values at 92°C (200°F) are used. The density of Holtite-A is assumed not to vary significantly from 92°C to its operational temperature limit. Recall that air properties are used above this limit to replace Holtite-A.

Deleted: 0

Comment [csb18]: This is not necessarily conservative for fire analyses. Recommend leaving the Holtite A intact for the duration of the fire and then substituting with air after the fire exposure.

Table IV-2. Thermal conductivities for the Rail-Steel materials.

Material	Thermal Conductivity W/m-°C (Btu/ft-hr-°F)				
	92°C(200°F)	226°C(450°F)	377°C(700°F)	477°C(900°F)	726°C(1340°F)
Air[§]	0.026 (0.015)	0.040 (0.023)	0.050 (0.028)	0.055 (0.031)	0.067 (0.038)
Stainless Steel[§]	14.5 (8.3)	18.3 (10.5)	20.4 (11.8)	21.9 (12.6)	25.4 (14.6)
Aluminum Alloy 1100[*]	228 (131)	212 (122)	—	—	—
Aluminum-Honeycomb[‡]	3.5 (2.0)	4.1 (2.4)	4.8 (2.8)	5.2 (3.0)	—
Boral (B_4C)[*]	83.3 (48.2)	83.1 (48.0)	81.3 (47.0)	80.5 (46.5)	—
Carbon Steel- Int. Shells[*]	42.3 (24.5)	41.7 (24.1)	38.8 (22.4)	—	—
Carbon Steel-N. Shield[*]	50.7 (29.3)	49.1 (28.4)	42.6 (24.6)	—	—
Cryogenic Steel[*]	41.1 (23.8)	41.0 (23.7)	38.5 (22.3)	—	—
Helium[§]	0.17	0.22 (0.12)	0.26 (0.15)	0.29 (0.16)	0.35 (0.20)
Holtite-A[*]	0.65 (0.37)	—	—	—	—
UO_2[*]	6.0 (3.4)	6.0 (3.4)	5.1 (2.9)	—	—
Zircaloy[*]	13.5 (1.78)	14.6 (8.4)	16.2 (9.3)	17.8 (10.2)	—

[§]Incropera and Dewitt, 1996
[*]Holtec International, 2004
[‡]Thermophysical Properties Research Laboratory Inc., 2001

Table IV-3. Specific heat for the Rail-Steel materials.

Material	Specific Heat J/kg-°C (Btu/lbm-°F)				
	92°C (200°F)	226°C (450°F)	377°C (700°F)	477°C (900°F)	726°C (1340°F)
Air[§]	1010	—	—	—	—
Stainless Steel[§]	482 (0.11)	535 (0.12)	563 (0.13)	575 (0.13)	611 (0.14)
Aluminum[§]	903 (0.21)	—	—	—	—
Aluminum-Honeycomb[‡]	890 (0.21)	976 (0.23)	1057	1100	—
Carbon Steel[§]	434 (0.10)	505 (0.12)	590 (0.14)	653 (0.15)	1169
Boral (B_4C)[*]	2478	—	—	—	—
Helium[§]	5193 (1.2)	—	—	—	—
Holtite-A[*]	1632	—	—	—	—
UO_2[*]	234	—	—	—	—
Zircaloy[*]	304	—	—	—	—

Comment [csb19]: Fix spacing, shading etc. to be sure that all tables are the same.

Formatted: Centered
Formatted Table
Deleted:
Deleted:
Deleted:
Deleted:
Formatted: Space After: 0 pt, Line spacing: single
Deleted:
Formatted: Centered, Space After: 0 pt, Don't adjust space between Latin and Asian text
Formatted: Centered, Don't adjust space between Latin and Asian text
Formatted: Centered, Don't adjust space between Latin and Asian text
Formatted: Centered, Don't adjust space between Latin and Asian text
Formatted: Centered, Don't adjust space between Latin and Asian text
Formatted: Centered, Don't adjust space between Latin and Asian text
Formatted: Centered, Don't adjust space between Latin and Asian text
Formatted: Centered, Don't adjust space between Latin and Asian text
Formatted: Centered, Don't adjust space between Latin and Asian text
Formatted: Centered, Don't adjust space between Latin and Asian text
Formatted: Centered, Don't adjust space between Latin and Asian text
Formatted: Space After: 0 pt, Line spacing: single

Table IV-4. Densities for the Rail-Steel materials.

Material	Density kg/m^3 (lbm/ft^3)				
	92°C (200°F)	226°C (450°F)	377°C (700°F)	477°C (900°F)	726°C (1340°F)
Air[§]	0.98	0.69	0.54	0.46	0.35
Stainless Steel[§]	7900 (493)	—	—	—	—
Aluminum[§]	2702 (168)	—	—	—	—
Aluminum-Honeycomb[‡]	526 (32)	—	—	—	—
Carbon Steel[§]	7854 (490)	—	—	—	—
Boral (B_4C)[*]	544 (34)	—	—	—	—
Helium[§]	0.14	0.10	0.077	0.065	0.048
Holtite-A[*]	1681 (105)	—	—	—	—
UO_2[*]	10956	—	—	—	—
Zircaloy[*]	6551 (409)	—	—	—	—

Table IV-5 shows the emissivity values obtained from Rail-Steel package SAR. The exterior surface of the Rail-Steel cask is coated with Carboline 890 paint and the overpack inner surfaces with Thermaline 450 paints, but these coatings are only good up to 216°C (422°F) and 262°C (505°F), respectively (Holtec International, 2004). Note also the internal surfaces of the heat conduction elements are sandblasted to increase radiation between opposite sides of the heat conduction elements.

Deleted: s

Table IV-5. Emissivity for some of the Rail-Steel materials and paints.

Material	Emissivity
Zircaloy	0.8
Painted Surface	.85
Rolled Carbon Steel	.66
Stainless Steel	.36
Sandblasted Aluminum	.40

IV.3.3.1 Effective Thermal Properties of Fuel Basket and Fuel-basket Periphery

Thermal properties for the fuel-basket region and fuel-basket periphery are obtained from the Rail-Steel SAR. In that report, the fuel basket and the fuel-basket periphery cross sections were replaced with two concentric cylinders each with equivalent effective thermal properties as described in Section IV.3.1.2. The procedure used to obtain the in-plane thermal conductivities

of the fuel basket and fuel-basket periphery as a function of temperature is described in this Rail-Steel SAR but is summarized here for completeness.

First, the cross section of the fuel assembly is modeled using a detailed two-dimensional, finite element model of the cross-section of a 17x17OAF fuel assembly rod arrangement (see Figure IV-5a), a uniform heat generation rate over each fuel rod, and a uniform temperature applied to the periphery of the fuel assembly. The 17x17OAF assembly used was determined to be the most resistive assembly design (Holtec International, 2004). The finite element model takes into account radiation between the rods and conduction across the helium gap. The effective thermal conductivity is obtained from the following equation:

$$k_{eff} = \frac{0.29468(q_g a^2)}{\Delta T}$$

where q_g is the heat generation rate per fuel cell per unit length, a is half the length of one side of the fuel cell, and ΔT is the maximum temperature difference in the fuel assembly (Sanders et. al., 1992). Since radiation is not linearly dependent on temperature, the model is run several times, each time with increasing uniform temperature near on the edge of the fuel assembly, to obtain effective properties at various temperatures. The detail fuel assembly is thus replaced with a homogenized fuel cell region (see Figure IV-6)

Second, the in-plane thermal conductivity of the basket storage wall, Boral, and stainless steel sheathing are replaced with an equivalent thermal conductivity using the thermal resistor network described in Rail-Steel SAR. The representative network takes into account the thermal resistances perpendicular to the wall and along the wall.

Third, the cross section of the MPC is modeled using a two-dimensional, finite element representation of the homogenized, fuel-basket walls, with a uniform heat generation rate applied over each homogenized fuel assembly, and a uniform temperature applied over the perimeter of the MPC shell. The model in the Rail-Steel SAR took into account: (1) conduction through the homogenized fuel assemblies, the helium gas in the flux traps, and the basket periphery, (2) radiation between homogenized basket walls, and (3) convection due to Rayleigh effects in the basket periphery. The effective conductivities of the basket region (k_b) and periphery region (k_p) are given by (Holtec International, 1999):

$$(k_b)_{eff} = \frac{Nq_g}{4\pi\Delta T_{bm}}$$

$$(k_p)_{eff} = \frac{Nq_g W}{A_s \Delta T_{pb}}$$

where

$$\Delta T_{pb} = \Delta T_{pm} - \Delta T_{bm}.$$

Here ΔT_{bm} is the maximum temperature difference in the basket, ΔT_{pm} is maximum temperature difference in the MPC cross section, A_s is the surface area per unit length, W is basket periphery annular gap length. The equivalent fuel-basket thermal conductivities are given in Table IV-6. The effective axial thermal conductivities of the fuel basket are obtained in the Rail-Steel SAR using the resistor method which reduces to an area weighted average since the basket length (L) in the resistance (L/kA) is equal across all materials. The specific heat and density are obtained using a mass and volume weighted average, respectively. Near the ends of the basket, the fuel rods are filled with gas, decreasing the in-plane and axial thermal conductivity of the basket slightly, since the thermal conductivity of helium is smaller than the UO_2 pellets. Note that the temperature conductivities vary very little in temperature.

The properties in Table IV-6 are used over the length of the basket. For consistency, temperature varying properties are implemented in the thermal model.

Fuel spacers separate the ends of the fuel assembly from the MPC lid and MPC bottom plate. In these regions, conduction is predominately through the helium gas, but thermal radiation occurs between the walls of the basket and the fuel spacers where the spacers overlap the fuel basket. Thus, outside the fuel rod region, the in-plane thermal conductivity is bounded by the thermal conductivity of helium and the effective conductivity of the active fuel-basket region. The in-plane, thermal conductivity is assumed to be the average of the helium conductivity and the fuel-basket region, homogenized conductivities. This in-plane thermal conductivity is varied to assess the sensitivity of this assumption; few were found, and did not have an impact at regions of interest (e.g., seals, cladding temperature, etc.) The axial thermal conductivity is obtained using an area weighted average using the dimensions of the basket, the fuel spacers, and the helium void. Dimensions for these components are provided in the Rail-Steel SAR. The specific heat and density in this region is obtained from a mass and volume weighted average, respectively, using the same components.

Deleted: .

Deleted: ,

Deleted: very little differences

Deleted: a

Comment [csb20]: This is a little confusing…what is not clear to me is what you actually modeled. Did you do the more detailed models as described in the HOLTEC SAR, in order to compare with your homogenized model results, or not?

Table IV-6. Effective thermal conductivity for the fuel-basket region.

Effective Thermal Properties	92°C (200°F)	226°C (450°F)	377°C (700°F)	477°C (900°F)	726°C (1340°F)
In-Plane Thermal Conductivity W/m-°C (Btu/ft-hr-°F)	1.9 (1.1)	2.6 (1.5)	3.4 (1.9)	—	—
Axial Thermal Conductivity W/m-°C (Btu/ft-hr-°F)	3.4 (1.9)	3.8 (2.2)	4.3 (2.5)	4.6 (2.6)	—
Specific Heat J/kg-°C (Btu/lbm-°F)	305 (0.073)				
Density kg/m^3 (lbm/ft^3)	2688 (168)				

Fourth, the thermal conductivity in the basket periphery is further enhanced to account for heat dissipation through heat conduction elements. The equivalent resistor network through the heat conduction elements is obtained using a two-dimensional, analytical model explained in the Rail-Steel SAR. This resistance is added in parallel with the resistance obtained from the two-dimensional, finite element model for the basket periphery region. The fuel-basket periphery, in-plane conductivity is given in Table IV-7.

Table IV-7. Effective thermal conductivity of the aluminum heat conduction elements.

Effective Thermal Properties	92°C (200°F)	226°C (450°F)	377°C (700°F)	477°C (900°F)	726°C (1340°F)
In-Plane Thermal Conductivity W/m-°C (Btu/ft-hr-°F)	0.43 (0.25)				
Axial Thermal Conductivity W/m-°C (Btu/ft-hr-°F)	10 (5.8)				
Specific Heat J/kg-°C (Btu/lbm-°F)	964 (0.23)				
Density kg/m^3 (lbm/ft^3)	132 (8.25)				

Formatted Table
Formatted: Centered, Space After: 0 pt
Formatted: Space After: 0 pt
Formatted: Centered, Space After: 0 pt
Formatted: Space After: 0 pt
Formatted: Centered
Formatted: Space After: 0 pt
Formatted: Centered, Don't adjust space between Latin and Asian text
Formatted: Space After: 0 pt

The axial thermal conductivity is obtained from an area weighted average using aluminum 1100 and helium properties. The area of the periphery region is given in Holtec International (1997). The area of the heat conduction elements is estimated at 3.5 times the fuel-basket, cell pitch (27.3cm [10.7in]), multiplied by the thickness of the elements (3.175mm [0.125in]) and the total number of aluminum inserts (8) (Holtec International, 1999). The specific heat and density of the fuel-basket periphery is obtained from an area and mass weighted average, respectively, again considering only aluminum 1100 and helium.

Heat transfer through the periphery region is further enhanced by radiation between the inner walls of the heat conduction elements and the walls of the MPC and fuel basket. The emissivity of stainless steel and sandblasted aluminum are not very different as observed in Table IV-6.

IV.3.3.2 Effective Thermal Properties of MPC-Overpack Helium Gap

In the horizontal position, the MPC rests on the overpack forming a non-concentric, variable-length, helium gap. This gap is not modeled explicitly. Instead, a two-dimensional, analytical model derived in Holtec International (1997) is used to obtain an effective conductivity through the variable-length gap. This model included the effects of the contact region as explained below.

To account for radial heat dissipation through the variable-length, helium gap and through the metal-to-metal contact area, equations for the overall heat conducted through these regions are summed and then equated to the overall heat conducted through a concentric gap to obtain an effective thermal conductivity for a constant-length helium gap (i.e., concentric gap). The

following equation taken from the Rail-Steel SAR is used to obtain the effective thermal conductivity across the gap (k_{gap}):

$$\frac{(k_{gap})_{eff}}{k_{gas}} = \frac{t}{\pi}\int_0^{\pi} \frac{1}{t(1-\cos\theta)+\varepsilon\cos\theta} d\theta$$

where k_{gas} is the conductivity of the gas, t is the thickness of the concentric gap and ε (0.5mm [0.02in]) is the metal-to-metal, contact area width. Results reported in the SAR show the effective conductivity through the equivalent concentric gap is twice the conductivity of helium.

IV.3.3.3 Effective Thermal Properties of Overpack Intermediate Shells

The Rail-Steel consists of a series of shell-gas layers between the inner shell wall and the outermost intermediate shell of the overpack. The contact gaps are assumed to be 0.05 mm (0.002in) across (Holtec International, 2004). No radiation is assumed through these gaps since radiation accounts for less than five percent of the effective conductivity for gaps of this size. The in-plane thermal conductivity is obtained by adding the resistances across each shell and gap in series. The axial and circumferential conductivities are assumed to be that of the shell layer material since the thermal conductivity of air and the gap area of air contribute very little. Similarly, the specific heat and density of the intermediate shell layers are assumed to be equal to the intermediate shell material.

Table IV-8. Effective thermal conductivity of the intermediate shells in the in-plane directions.

Effective Thermal Properties	92°C (200°F)	226°C (450°F)	377°C (700°F)	477°C (900°F)	726°C (1340°F)
In-Plane Thermal Conductivity W/m-°C (Btu/ft-hr-°F)	13.2 (7.6)	15.6 (9.0)	17.0 (9.8)	18.6 (10.7)	22.1 (12.7)

IV.3.3.4 Effective Thermal Properties of Neutron Shield Region

The neutron shield region consists of the Holtite-A inside the cavities formed between the outermost intermediate shell and the outer enclosure shell, and between the radial channels. Note the outer enclosure shell is not included here since it is modeled explicitly. The neutron shield region includes the Holtite-A material and the radial sections of the channel (2 per channel for a total of 40). This region is also modeled as a single volume with homogenized thermal properties.

Table IV-9 shows the effective properties in the neutron shield region. The effective thermal conductivity in the in-plane and axial direction are obtained by summing the resistance through the radial channels and through the neutron shield material in parallel. Since both the Holtite-A

and radial channels extend the same length in the axial direction, the resistance equation in the axial direction reduces to an area weighted average of the individual material conductivities.

Table IV-9. Effective conductivity of the neutron shield region.

Effective Thermal Properties	92°C (200°F)	226°C (450°F)	377°C (700°F)	477°C (900°F)	726°C (1340°F)
In-Plane Thermal Conductivity W/m-°C (Btu/ft-hr-°F)	4.3 (2.4)	3.5 (2.0)	3.2 (1.8)	3.1 (1.8)	2.7 (1.5)
Axial Thermal Conductivity W/m-°C (Btu/ft-hr-°F)	3.6 (2.0)	3.3 (1.9)	3.0 (1.7)	3.0 (1.7)	2.6 (1.5)
Specific Heat J/kg-°C (Btu/lbm-°F)	1315 (0.31)	505 (0.12)	590 (0.14)	653 (0.15)	1170 (0.28)
Density kg/m^3 (lbm/ft^3)	2113	552 (34)			

The thermal conductivity in the circumferential direction is assumed to be that of Holtite-A since the total thickness of the radial channels in this direction is small compared to the total circumferential length of the Holtite-A. Note that this is a conservative assumption in the sense that heat dissipated through the neutron shield region is preferentially in the in-plane and axial directions as a result of the latter assumption. This assumption does not have an impact in the uniform heating run, but it does have impact on the CAFE-fire runs, where heat input around the circumference of the cask varies. In this case, heat will be dissipated more readily through the in-plane direction; thus giving higher temperatures in the interior of the cask.

Deleted: to

The specific heat and density of the neutron shield region are obtained using a mass and area weighted average, respectively. Holtite-A is expected to reach its temperature limit during the early transient period of a fire. When this happens, Holtite-A partially decomposes leaving char residue behind. Most of the excess gas generated in Holtite-A outgases through the rupture disks when the pressure inside the neutron shield region reaches the disks design limits. In the thermal model, when Holtite-A temperature limit is reached, Holtite-A is replaced with air, and radiation is activated by setting the emissivity to an appropriate value. Note that air effectively lowers the specific heat and density of the neutron shield region. The effective specific heat of the neutron shield region is greatly influenced by the specific heat values of carbon steel since the density of air in the mass weighted average is very small compared to carbon steel.

IV.3.4 Rail-Steel P-Thermal Finite Element Model and Boundary Conditions

A steady-state case is run to obtain the initial conditions of the Rail-Steel cask and to compare results against those provided in the Rail-Steel SAR and in Adkins et. al. (2006). The steady-state model consisted of the Rail-Steel cask being exposed to a 37.8°C (100°F) ambient temperature, radiation boundary condition. This boundary condition is applied over the entire outer surface of the package using an emissivity of 0.85. In addition, insolation is applied over

the outer curved surfaces of the package (193.8W/m^2 [34.1 Btu/ft^2-hr-°F]) and over the flat ends of the package (96.9W/m^2 [17.0 Btu/ft^2-hr-°F]) as specified in (ASTM E 2230). A convection boundary condition is also applied to the outer surface of the package using a heat transfer coefficient of 3W/m^2 (5 Btu/ft^2-hr-°F). This value is obtained from a set of correlations described in the Rail-Steel SAR—assuming turbulent flow—and is within the same order of magnitude as values obtained from correlations in (Incropera and Dewitt, 1996).

In general steady-state results are slightly higher than those presented in the Rail-Steel SAR, but lower than those reported in Adkins et. al. (2006). For example, the current study found a maximum fuel cladding temperature of 376°C (710°F), compared to 372°C (701°F) in the Rail-Steel SAR and 392°C (738°F) in Adkins et. al. (2006). The largest differences are observed in the extreme ends of the overpack, where temperatures in the Rail-Steel are lower (by ~25°C) than reported here and significantly lower (~50°C) than what is reported in Adkins et. al. (2006). These differences are attributed to dissimilarities in modeling assumptions and approaches, and boundary conditions. For example, in Adkins et. al. (2006) a gap is assumed between the overpack and the limiters. Overall, however, the temperatures obtained from these three studies showed similar spatial trends and good agreement given the differences cited above.

The steady-state case is used to assess the suitability of the mesh. The mesh is initially 169600 elements; this corresponded to a nominal element size of 10.2cm (4in). This value is decreased to 5.1cm (2in) and then increased to 15.2cm (6in) to study the effects of element size on temperatures at locations of interest (as shown in the results of Chapter 4 and later in this Appendix). Results of the 15.2cm, element-size mesh showed some difference in the temperatures in the interior of the package when compared to those of the 10.2cm, element-size mesh. This is expected since large cells are created in the interior of the package. Near the exterior of the overpack, small geometric features resulted in small size elements. Results of the 5.1cm, element-size mesh showed very little difference when compared to the 10.2cm element mesh. The 5.1cm, element-size mesh had smaller elements in the interior and about the same near the exterior of the overpack. Therefore a third case is run, this time using the 10.2cm mesh, with a refined mesh in the near the exterior of the overpack. Results from this mesh showed some difference (less than 5 degrees in the neutron shield region), but not enough to justify the extra computational time needed to run this mesh. Figure IV-8 shows the final mesh used to run the five scenarios described in Chapter 4.

Comment [csb21]: I would list this and any other sensitivity studies done for this report in a table for easier consumption.

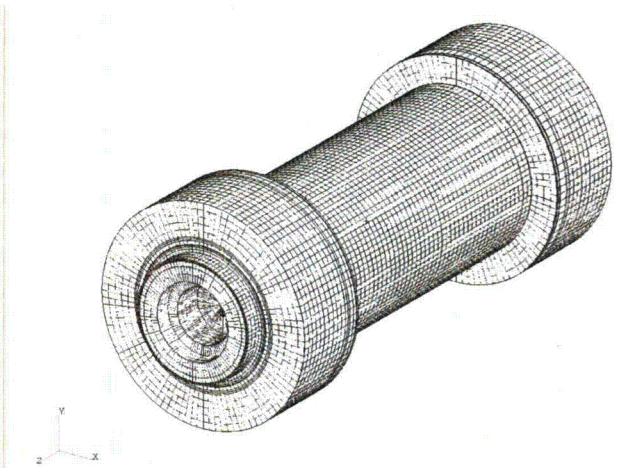

Figure IV-8. Rail-Steel finite element mesh.

Comment [csb22]: Could you provide a cross section of this package model?

The uniform heating case described in Chapter 4 is run initially to verify the Rail-Steel FE model. This exercise gave an additional measure of confidence in the Rail-Steel model. The boundary conditions for this case consisted of the Rail-Steel cask being exposed to an 800°C (1472°F) ambient-temperature, radiation boundary condition. This boundary condition is applied over the entire outer surface of the package using an emissivity of 0.9. A convection boundary condition is also applied to the outer surface of the package using a heat transfer coefficient of $85 W/m^2$ (15.2 Btu/ft^2-hr-°F). This value is obtained in the Rail-Steel SAR from a set of correlations described there and assuming a 15m/s (49ft/s) vertical flame speed, a value significantly higher than what is specified in Nakos (2005) but nevertheless conservative in that it will result in a higher heat input to the cask. Convection accounts for about 10-20% of the total heat input for large objects inside a fire, the rest is through thermal radiation (Nicolette and Larson, 1989).

The uniform heating case is run for 30 minutes, followed by an 11.5 hour transient cool down. During the cool down period, the boundary conditions are set back to their steady-state case values, except for the emissivity of the outer cask which remained the same to simulate what happens in actual fires—a blanket of soot covers the cask. Also, the neutron shield region is assumed to contain air with radiation interaction between the outer enclosure shell and the outermost intermediate shell.

Overall, maximum temperatures obtained using the model developed here and in the Rail-Steel SAR show some differences during the 30 minute fire and during the cool down period—6% or less lower through the cask cross section, and 20% lower in the closure plate seal region. This

Comment [csb23]: Does this mean that the models you have generated are non-conservative?

difference can be attributed to significant differences in boundary conditions. During the fire, the impact limiters are assumed to have been crushed. This effectively reduces the lateral dimension of the cask and increases the thermal conductivity through the limiters. Moreover, during the cool down period, a smaller emissivity value is assumed and no credit is taken for conduction through the neutron shield material (i.e., Holtite-A region). In this study, the most realistic boundary conditions are used, which were not necessarily the most conservative in terms of heat input. Only when reliable data was not available, or when current tools did not allow for effective implementation of realistic boundary conditions are conservative assumptions applied.

For the remaining cases, the external boundary conditions are obtained from CAFE, the computational fluid dynamics code coupled to P-Thermal. As is mentioned in Section IV.2, a boundary condition is setup in PATRAN that allowed CAFE results to be communicated to P-Thermal and vice-versa. The cool down period for these cases also used the steady-state case boundary conditions (from 10 CFR 71.71).

Deleted: ,

IV.3.5 Rail-Steel Thermal Analysis Results

Pages 32 through 41 show results for the five scenarios already described in Chapter 4. These results are not discussed here, but are presented to supplement results discussed in Chapter 4r. Figure IV-9 shows results for the regulatory uniform heating case cited in the previous section. This is the P-Thermal only run. Figure IV-10 shows results for the regulatory CAFE fire and together with Figure IV-9 may be useful in determining the differences between uniform and non-uniform fire conditions. The effect that large objects have on fires and their implications to modeling large packages in fires has been discussed in Nicolette and Larson (1989). Figure IV-11 shows results for the fully engulfing CAFE fire with the cask on the ground, and Figures IV-12 and IV-13 show results for the cask on ground but outside the fire. The last three cases are for a three hour fire and subsequent cool down period.

IV.4 RailPackage with Lead Shielding

Deleted: -Pb

The Rail-Pb (Nuclear Acceptance Corporation International, 2004) is also certified to transport spent nuclear fuel material in rail cars. This cask is chosen because it presents quite a different design philosophy from the Rail-Steel cask. The Rail-Pb cask uses lead for the gamma shield. Morevoer, the Rail-Pb package carries SNF without a separate Multi Purpose Canister. As in the Rail-Steel analysis, the Rail-Pb is assumed to be in the horizontal configuration, as it would be during transportation, and most likely after an accident scenario. Only the thermally relevant components of the Rail-Pb are considered to estimate the thermal response of this cask.

Deleted: cask is able to carry

Deleted: spent fuel

Deleted: the need for

Deleted: MPC

Deleted: c

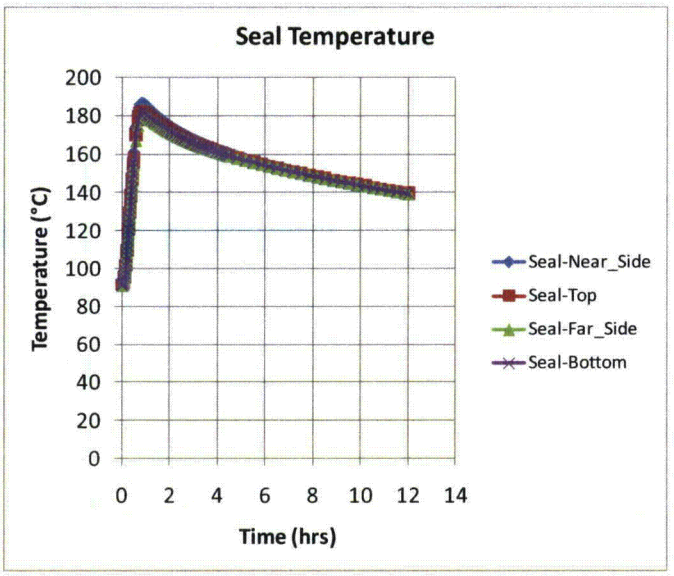

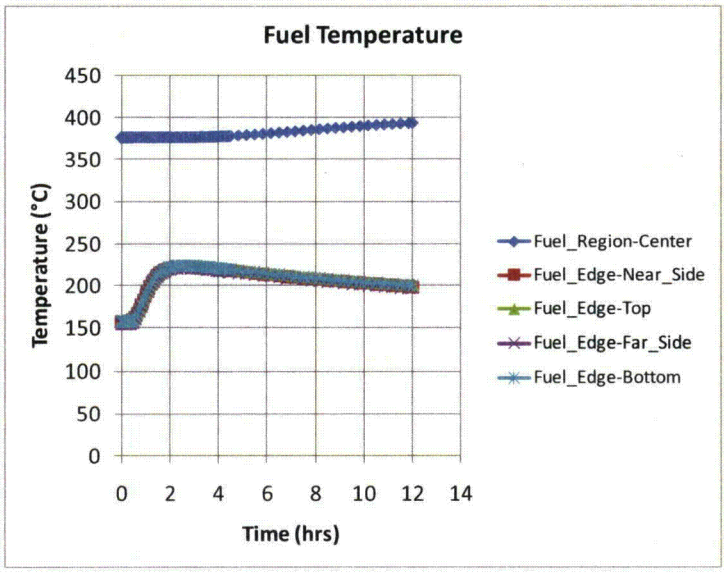

Figure IV-9. Rail-Steel Regulatory Uniform Heating Results (P-Thermal)

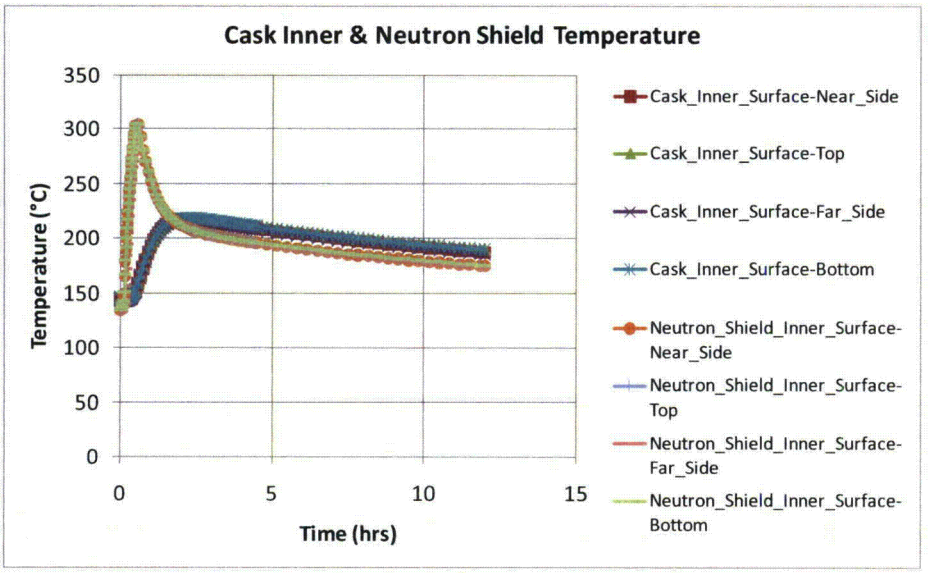

S

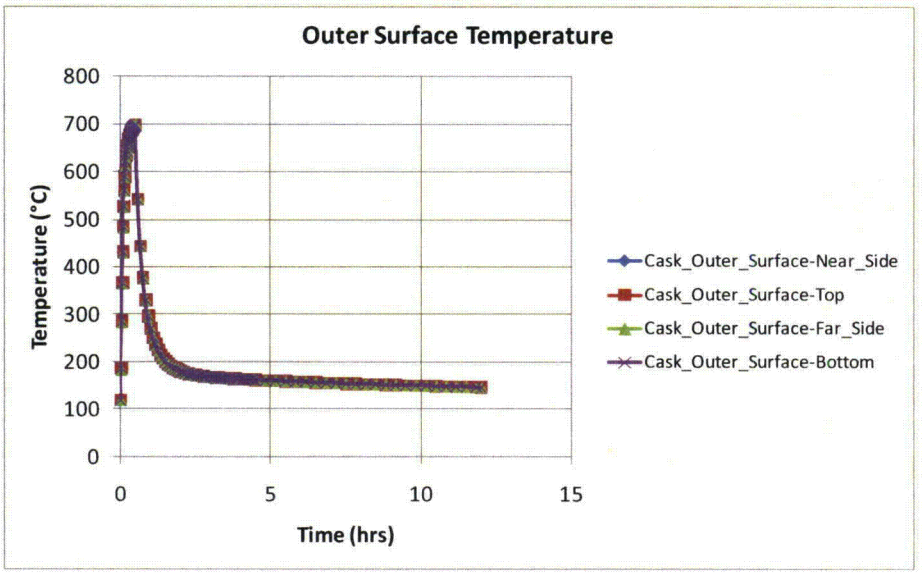

Figure IV-9. Rail-Steel Regulatory Uniform Heating Results (P-Thermal) – Continue

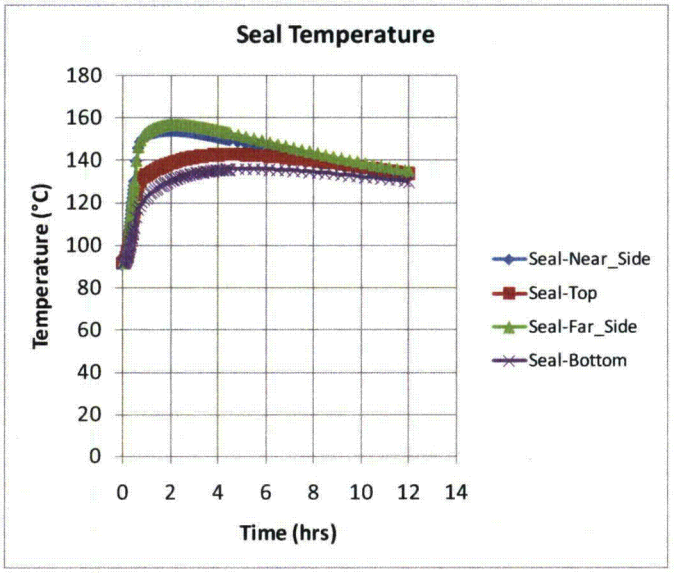

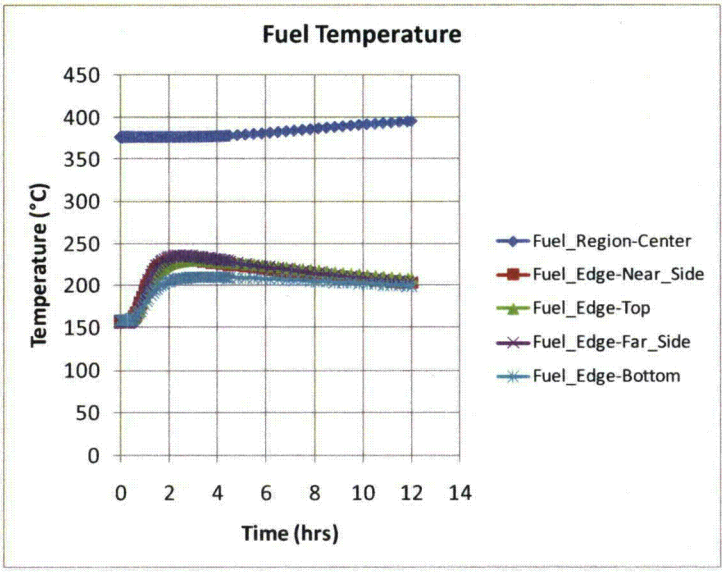

Figure IV-10. Rail-Steel CAFE regulatory fire.

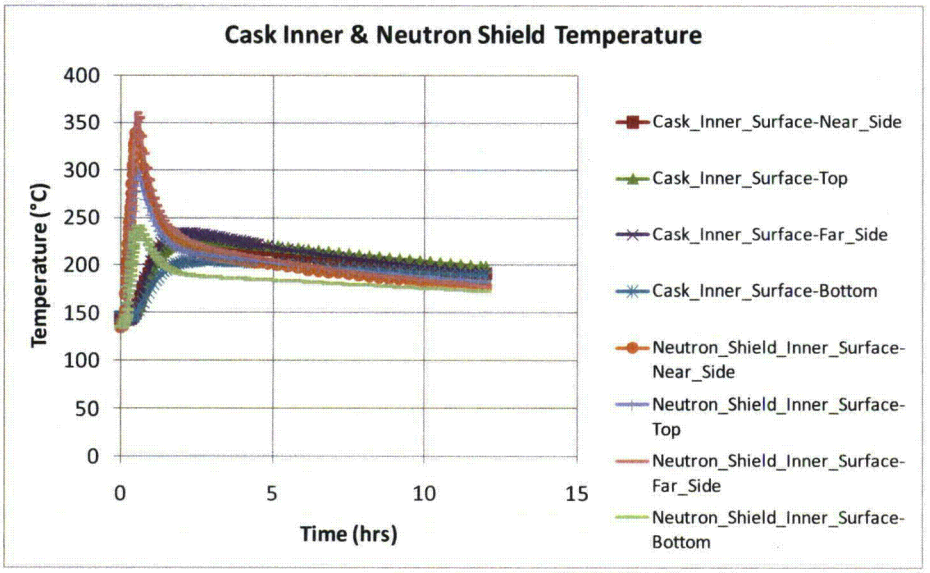

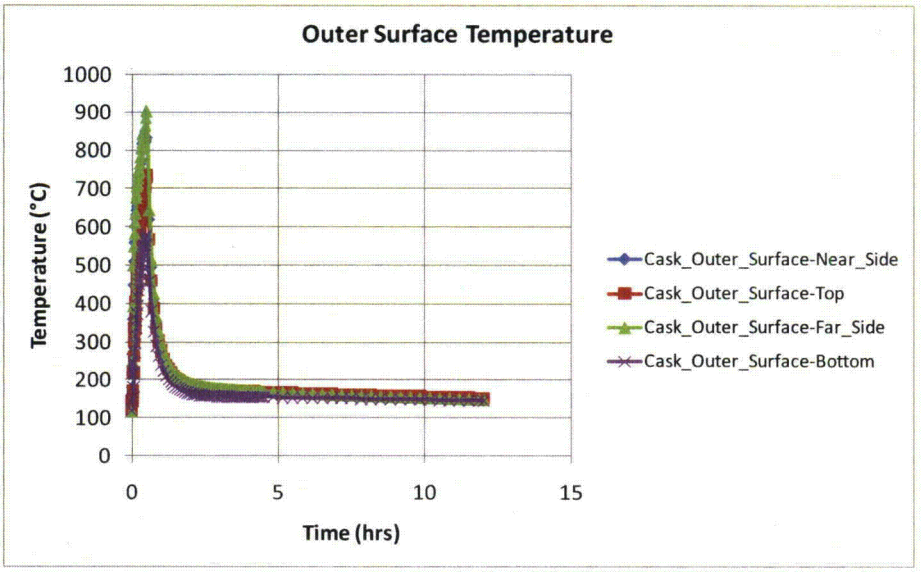

Figure IV-10. Rail-Steel CAFE regulatory fire. – Continue

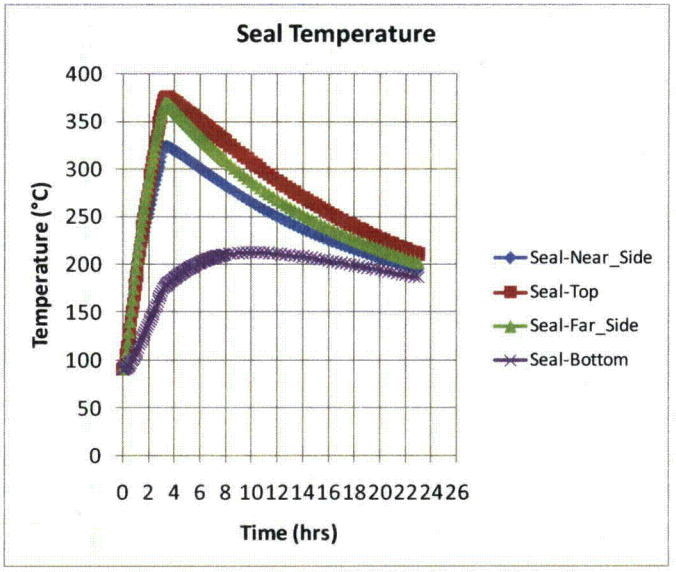

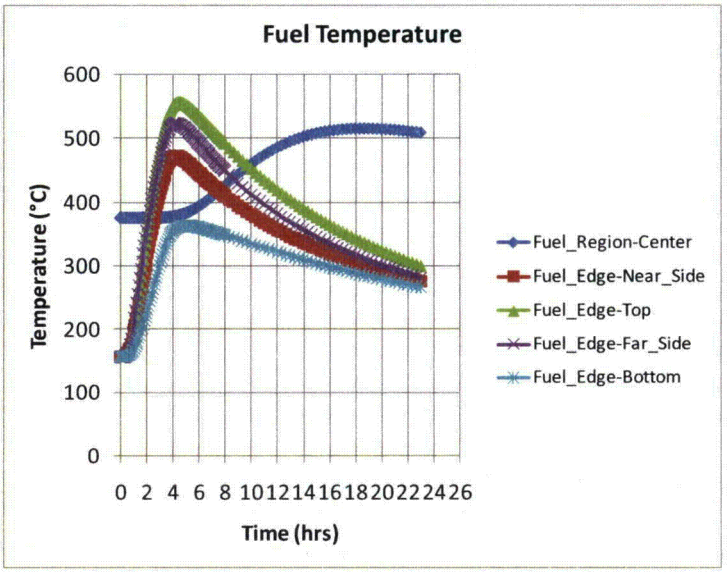

Figure IV-11. Rail-Steel CAFE fire with cask on ground and at the pool center.

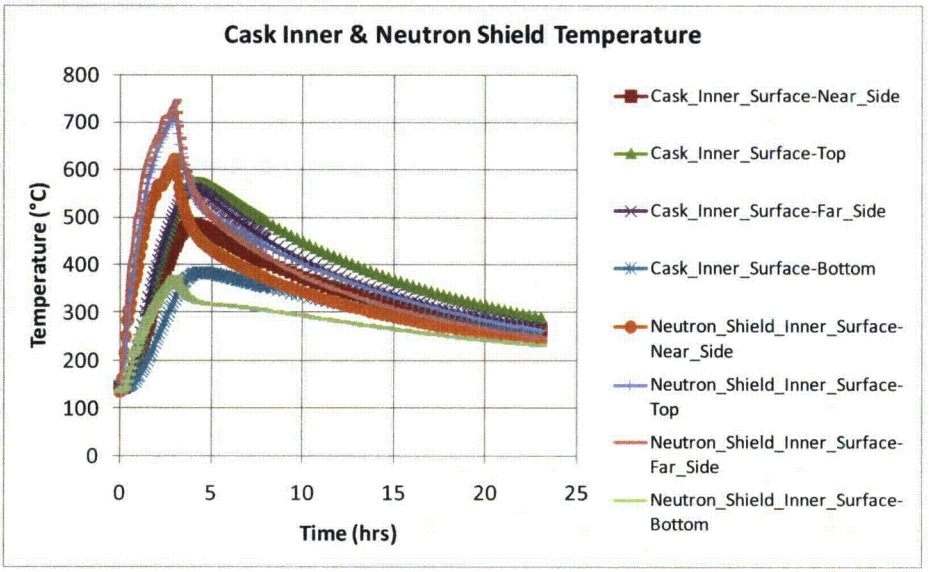

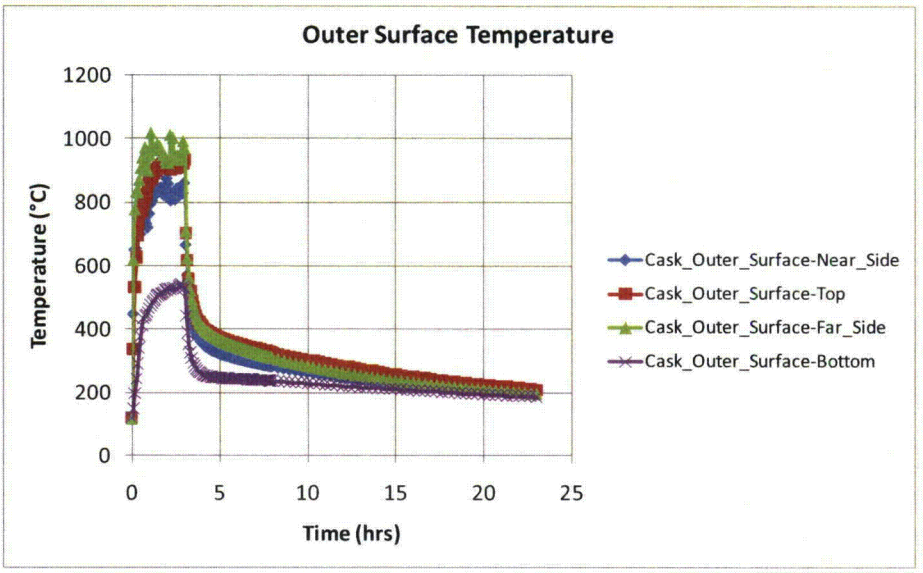

Figure IV-11. Rail-Steel CAFE fire with cask on ground and at the pool center. – Continue

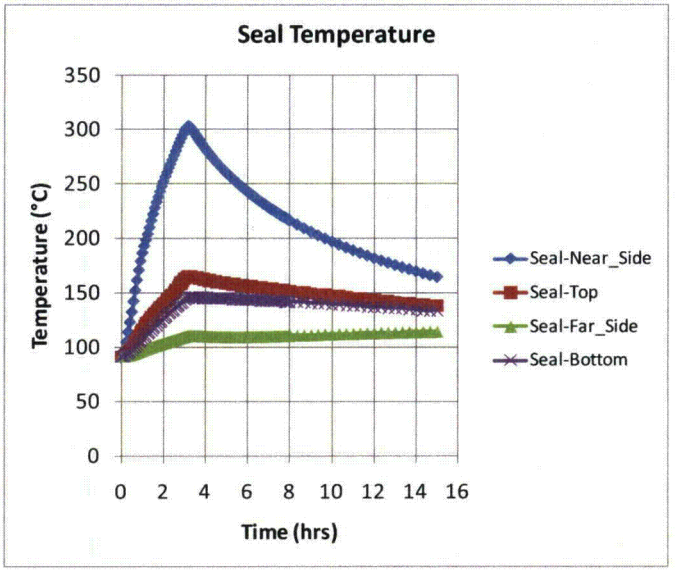

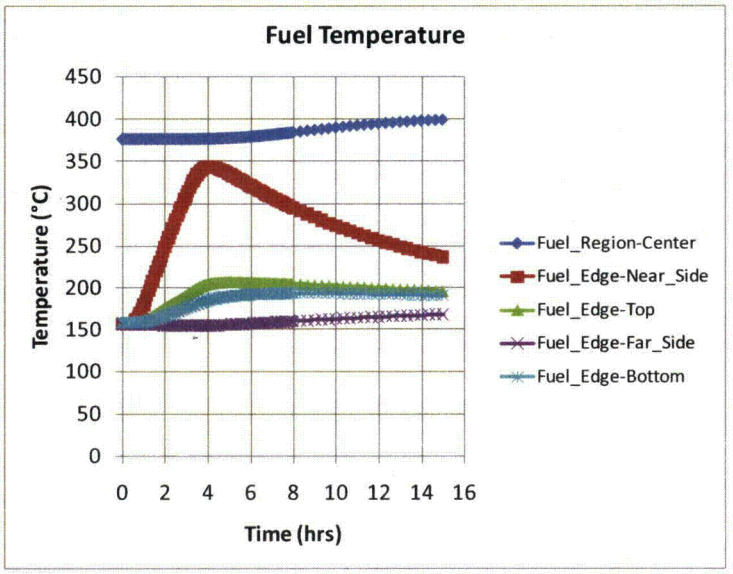

Figure IV-12. Rail-Steel CAFE fire with cask on ground 3.0m (10ft) from the edge of the pool.

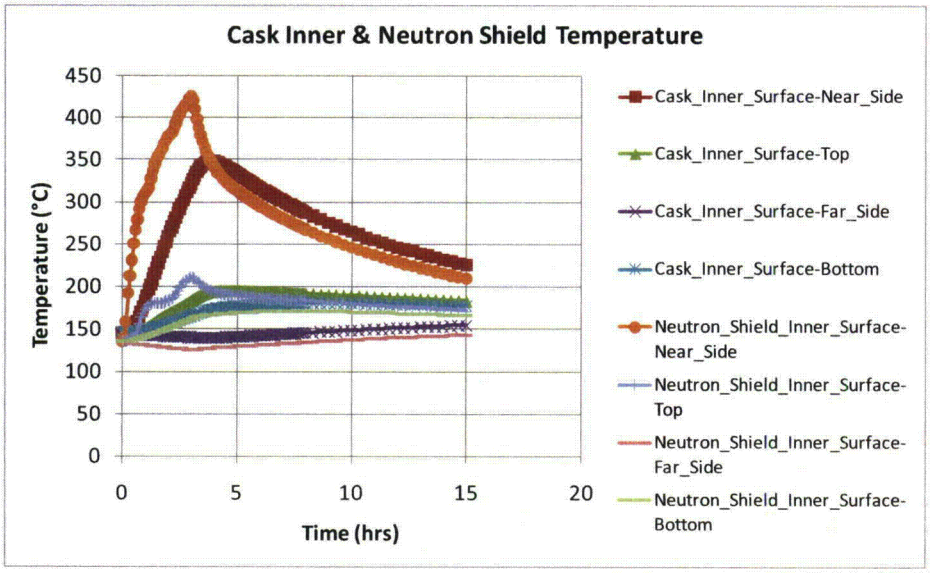

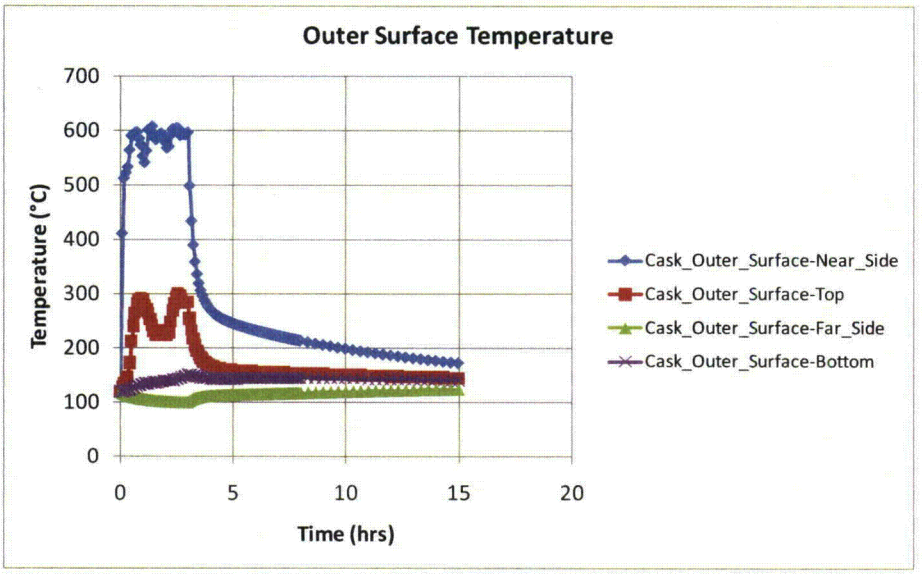

Figure IV-12. Rail-Steel CAFE fire with cask on ground 3.0m (10ft) from the edge of the pool. - Continue

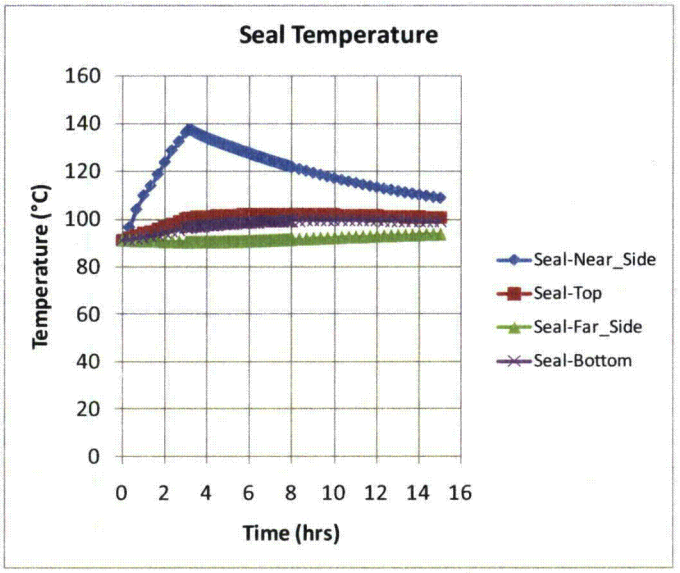
Seal Temperature
Temperature (°C)
160
140
120
100
80
60
40
20
0
0 2 4 6 8 10 12 14 16
Time (hrs)
Seal-Near_Side
Seal-Top
Seal-Far_Side
Seal-Bottom

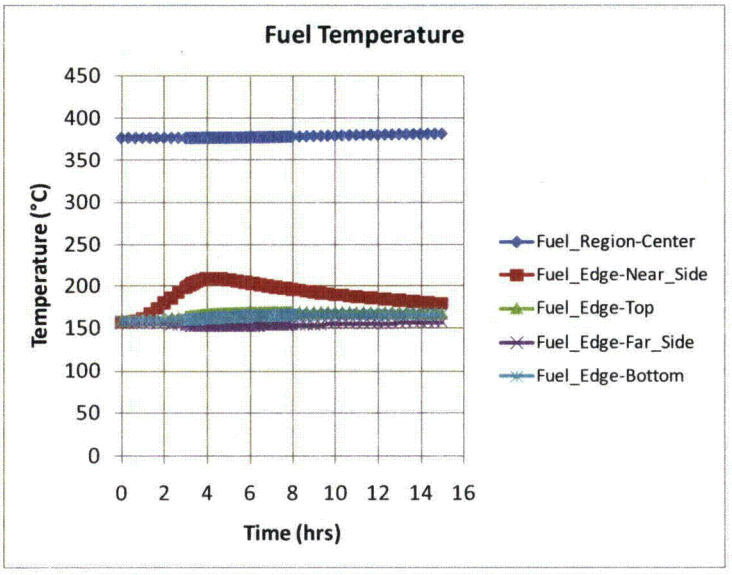
Fuel Temperature
Temperature (°C)
450
400
350
300
250
200
150
100
50
0
0 2 4 6 8 10 12 14 16
Time (hrs)
Fuel_Region-Center
Fuel_Edge-Near_Side
Fuel_Edge-Top
Fuel_Edge-Far_Side
Fuel_Edge-Bottom

Figure IV-13. Rail-Steel CAFE fire with cask on ground 18.3m (60ft) from the edge of the pool.

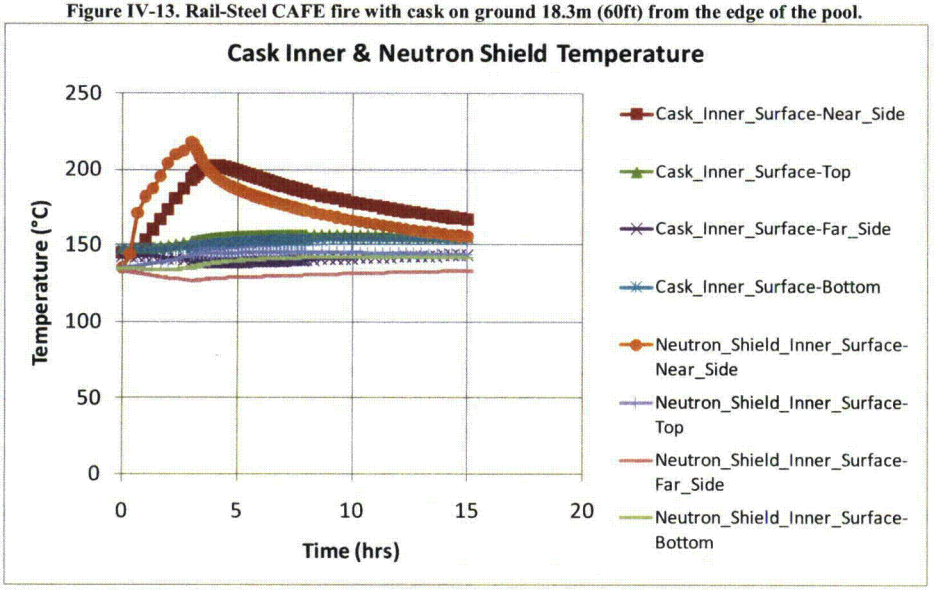

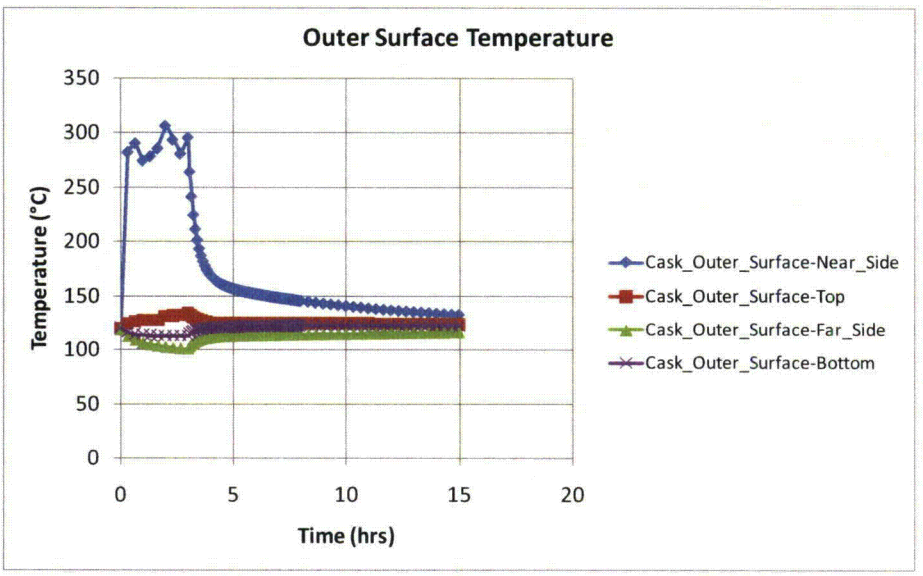

Figure IV-13. Rail-Steel CAFE fire with cask on ground 18.3m (60ft) from the edge of the pool. – Continue

The Rail-Pb package uses a single lead gamma shield as opposed to a multilayer carbon steel gamma shield like the one used in the Rail-Steel cask. This lead shield melts at relatively low temperatures, but remains in the overpack in molten form until the temperature is low enough to change back to the solid state. This process has an impact of the cask ability to attenuate gamma rays as described in Chapter 5 and Appendix V. One unique feature of the Rail-Pb cask is that it can store the spent nuclear fuel in a directly loaded fuel basket in addition to inside an MPC as is seen in the Rail-Steel package. The directly loaded configuration is a significant design departure from the MPC configuration since there is no barrier between the fuel assemblies and the inner walls of the overpack. For this reason, this analysis focuses on the directly loaded configuration. Finally, the Rail-Pb uses wood filled impact limiters as oppose to an aluminum honeycomb, a minor difference from the thermal analysis point of view, but nevertheless important to point out.

Deleted: cask

Deleted:

Comment [csb24]: Is this true…it can take an MPC as well?

In most cases, results reported in the Rail-Pb SAR (Nuclear Assurance Corporation International, 2004) are used but modified where necessary as is done with the Rail-Steel analysis. The only significant departure is how the interior of overpack is treated in the Rail-Pb SAR as explained in the introduction of this Appendix. Unlike the method used in that SAR, the directly loaded basket is replaced with a cylinder having equivalent effective thermal properties using a simple, three-dimensional, finite element model and the thermal resistor network method. As is done in the Rail-Steel analysis, the neutron shield region is replaced with an equivalent thermal region using the thermal resistor network method. The impact limiters are also modeled in the uncrushed state for the same reasons cited in Section IV.3.1.3.

Deleted: Acceptance

IV.4.1 Geometry Considerations

The directly loaded Rail-Pb cask consists of an overpack, a fuel basket, and limiters at each end of the basket as shown in Figure IV-14. The directly loaded fuel basket is an open fuel container designed to fit snug within the overpack interior cavity. The overpack is designed to attenuate both the heat, and the neutron and gamma rays generated inside the fuel basket. The overpack contains two lids, each fitted with seals that completely seal the contents inside the overpack from the outside environment. This double lid design essentially forms a double containment barrier. The total length of the Rail-Pb, including the limiters, is approximately 6.5m (256 in).

Comment [csb25]: Not necessarily…I would not use the word double containment.

IV.4.1.1 Overpack

The Rail-Pb overpack is also a multilayer cylindrical vessel approximately 2.20m (86.7in) in diameter and 4.90m (193in) in length (see Figure IV-14). The inner cavity of the overpack is approximately 1.80m (71in) in diameter and 4.19m (165in) in length. The cross section of the overpack vessel is made of three shells layers arranged in following order starting from the center of the overpack: an inner shell, a lead shell, and an outer shell (see Figure IV-15). As in the Rail-Steel cask, these shells are tightly coupled to each other and are welded to the overpack bottom plate and top flange. The lead shell acts as the gamma shield in this design. The thickness

of the inner shell wall is not constant throughout, but tapers in slightly through most of the overpack side wall. That allows the thickness of the lead shell to increase slightly through the

Deleted: ¶

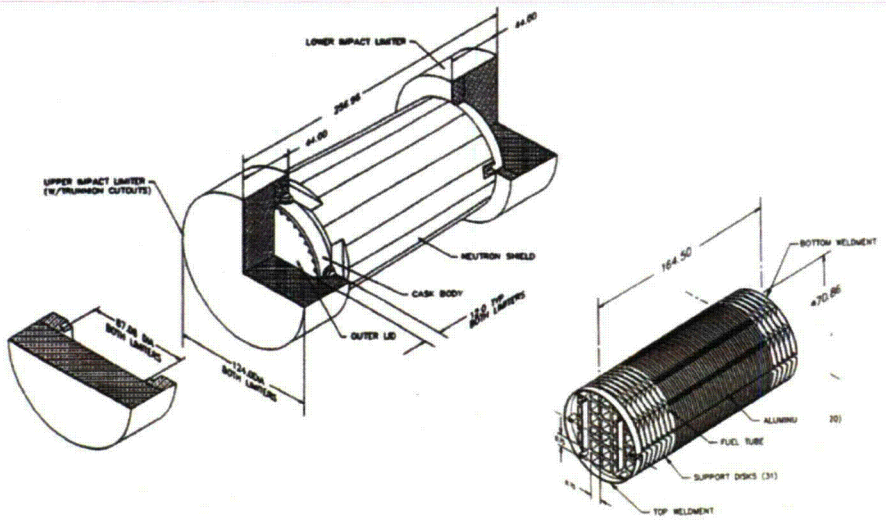

Figure IV-14. Rail-Pb components with the direct loaded fuel basket shown to the right.

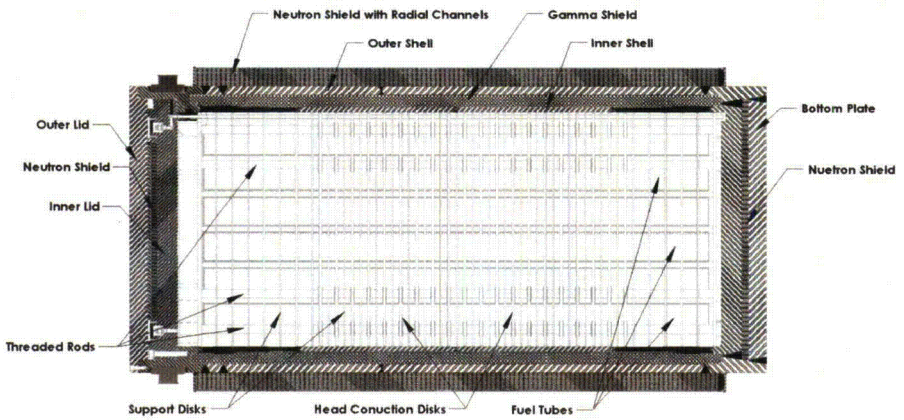

Figure IV-15. Cross-section view of the Rail-Pb with the directly loaded fuel basket.

same section of the overpack, where the gamma shielding is most needed. Radial channels are also welded to the outer shell to enhance heat transfer through the neutron shield region. The outer enclosure shell is formed the same way as in the Rail-Steel. Similarly, the cavities formed by the outer enclosure shell, the radial channels, and the outer enclosure shell are filled with a neutron shield material. The neutron shield region increases the diameter of the overpack an additional 29.2cm (11.5in). Unlike the Rail-Steel, the overpack contains inner and outer lids that fit into the vacuum flange and complete the double containment barrier. Both the inner lid and bottom plate contain 5cm (2in) thick cylindrical layer of neutron shield within them.

Deleted: ¶

The inner, outer, and lead shells, the vacuum flange, the inner and outer lids, and the bottom plate are represented explicitly in the thermal model with minor alterations to simplify the model. The most significant change is making the thickness of the inner shell and lead shell constant throughout. Their thickness is kept equal to the corresponding thicknesses in the middle section of the overpack. As in the Rail-Steel model, the neutron shield region is represented as a single volume to minimize geometric complexity. As with the Rail-Steel, the Rail-Pb overpack contains a number of features that serve a special purpose. These features are omitted from the model as is done in the Rail-Steel model and for the same reasons: (1) negligible due to their small volume and mass relative to the other components in the overpack, (2) highly localized with no effect to the overall thermal performance of the package at locations of interest, or both.

IV.4.1.2 Directly Loaded Fuel Basket

In the Rail-Pb, the nuclear spent fuel is stored in a directly loaded basket (see Figure IV-14). In this configuration, the fuel basket can store up to 26 PWR fuel assemblies. The total length of the fuel basket is 4.18m (164.5in) and the diameter is a little less than the inner diameter of the overpack. The fuel basket consists of thirty-one support disks and twenty heat transfer disks, aligned parallel to each other, and each precisely separated using six threaded rods and spacer nuts. The heat transfer disks are placed between the support disks in the region where the heat decay rate is at a maximum. Except for the end support disks, all support disks are the same thickness; the end support disks are twice as thick. Except for the end support disks, all heat transfer disks are slightly thicker. Both disk types contain twenty-six square holes spaced at regular intervals, and aligned between disks. Each square hole fits a thin walled, square, fuel tube which extends almost the length of the basket. These tubes are welded to the disks and accommodate the fuel assemblies. The fuel assemblies extend almost the entire length of the fuel basket. The basket active fuel region is assumed to be 3.66m (144in) in length as suggested in the Rail-Pb SAR. Additional plates and a short length cylinder are welded to the end support disks for extra support and complete the fuel-basket design. The fuel basket fits within the inner cavity of the overpack, but there are a small gap between the basket disks and the inner wall of the overpack, and between the ends of the basket, and the lid and bottom plate walls.

As in the Rail-Steel, each fuel assembly consists of an array of fuel rods, each separated by a helium gas space. The total number of rods in the fuel assembly, the dimensions of each rod, and

the type of fuel cladding vary between assembly designs. A more complete description of the fuel assembly and fuel rods is given in Section IV.3.1.2.

The fuel basket and fuel assemblies are not explicitly included in the model. Instead, a separate three-dimensional model is generated to obtain the effective properties of the basket in the in-plane and axial directions. Since the basket support disks, gas regions, and heat transfer disks repeat at regular intervals in the active fuel region, a three-dimensional, quarter solid model of a section comprising two support disk, heat transfer disk, and the gas and fuel tubes between them is generated to obtain the effective properties of the basket in the in-plane and axial directions. The diameter of the support and heat transfer disks is assumed the same to simplify the solid modeling and mesh process. The same model is used for the portion of the fuel basket without the heat transfer disk. In this case, the material properties and boundary conditions for the heat transfer disk are replaced with those of the gas region.

IV.4.1.3 Impact Limiters

The impact limiters in the Rail-Pb are cylindrical wood-filled structures also encased in a thin metal shell. Each impact limiter is 3.15m (124in) in diameter and 1.12m (44in) in length (see Figure IV-14). The depth of the cap where the overpack fits is 30.5cm (12in.). These limiters serve the same purpose as the impact limiters in the Rail-Steel (see Section IV.3.1.3). Since the impact limiters are mostly wood and have very little metal structures, they are modeled as two coupled solid wood structures, retaining their volume and shape.

IV.4.2 Rail-Pb Thermal Behavior and Model Assumptions

The Rail-Pb package is also designed to release heat passively under normal conditions of transport. In the direct loaded configuration, the basket is designed to accomodate a maximum heat load of 22.1kW (0.85kW per fuel assembly). Figure IV-16 shows the normalized, axial heat generation rate distribution for a typical PWR assembly. As with the Rail-Steel, heat is dissipated from the fuel rods to the exterior surfaces of the Rail-Pb by a combination of conduction, convection, and radiation heat transfer.

Deleted: by passive means

Deleted: generate at most

Deleted:

Comment [csb26]: Assemblies heat generation rates are not cask-specific.

Deleted: Rail-Pb

Deleted: modes

The fuel assembly design in the Rail-Pb is conceptually the same as in the Rail-Steel model; therefore, the same heat transfer mechanisms are present as described in Section IV.3.2. The approach described in Section IV.3.3.1 is also used in Rail-Pb SAR to obtain the effective thermal conductivity of the fuel assembly in radial direction. Values presented in the Rail-Pb SAR are used in this study and are not much different from what is used in the Rail-Steel SAR, as expected. Heat from generated in the assembly is dissipated by conduction through the fuel tube walls. From the tubes, heat is then radially dissipated by conduction through the support and heat transfer disks, and through the gas in the void formed between the tubes and the inner wall of the overpack; and by radiation to the adjacent tubes and disks, and to the inner wall of the overpack. Convection due to Rayleigh effects is also possible in the gas void. As in the Rail-Steel fuel basket, convection is limited to a few regions around the basket perimeter. However, unlike the HI-STAR configuration, the convective cells in the Rail-Pb basket are confined to the

Comment [csb27]: Unless the package is horizontal.

gas void between adjacent disks. Moreover, heat dissipated from the adjacent disks through this void tends to decrease the temperature gradient across this void region, reducing temperature gradient induced flow. In the Rail-Pb model, convection is neglected in this region since it is not expected to be significant given the Nusselt values presented in the Rail-Steel SAR for a similar void configuration.

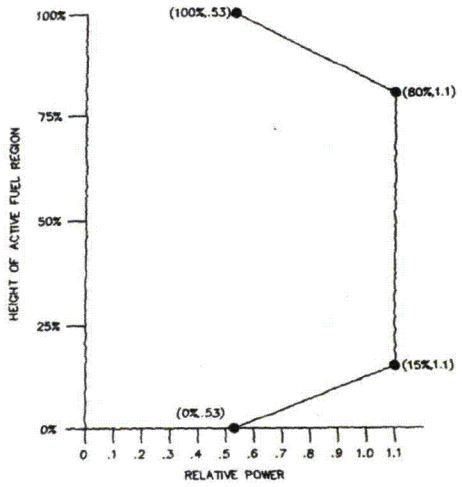

Figure IV-16. Axial burn up profile for the directly loaded fuel basket.

Heat is dissipated radially by conduction and radiation through the gap between the disks and the overpack inner wall. This gap is assumed to be 1.65mm (0.065in) across as stated in the Rail-Pb SAR. As mentioned before, a three-dimensional, quarter section of the fuel basket is generated to obtain effective thermal conductivities in the in-plane and axial directions (see Figure IV-17). The small gap between the disks and the inner wall of the overpack is included (not clearly visible in Figure IV-17). Except for convection, all modes of heat transfer are accounted for in this model, and included radiation between the tubes, between the tubes and the disks, between the tubes and the inner shell (also not shown), between the disks, and between the disks and the inner shell (not shown?). In the horizontal position, the disks make contact with the inner shell wall. To account for conduction through the contact area between the disks and the inner shell wall, the same model derived in Holtec International (1997) is employed to enhance conductivity through the equivalent concentric gap (see Section IV.3.3.2). Note that both the support and heat transfer disk diameters are assumed to be the same after thermal expansion.

Heat transfer through the inner shell?, lead, and outer shell of the overpack occurs by conduction through the shell materials. These are modeled explicitly. As in the Rail-Steel, conduction in the neutron shield region occurs in parallel through the radial connectors and the neutron shield material.

Heat transfer from the cross section of the direct loaded basket and overpack to the axial ends of the overpack is assumed to occur by conduction and radiation. Heat conduction occurs in parallel through each of the connecting materials that comprise the basket and overpack. The effective thermal properties are obtained in the same manner as in the Rail-Steel model. Radiation is assumed to occur between the end disks of the basket to the interior wall of the inner lid and bottom plate of the overpack.

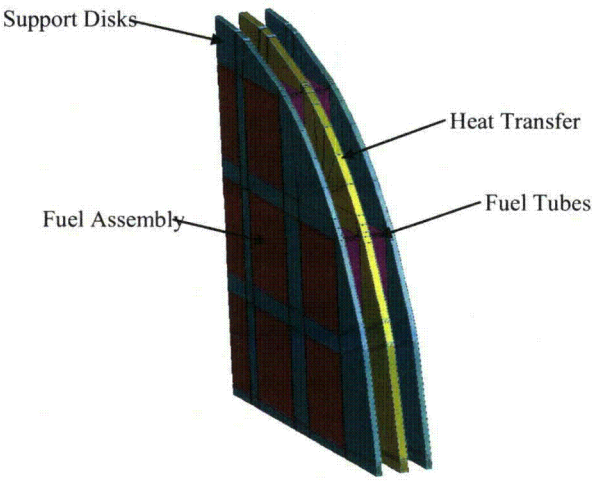

Figure IV-17. Three-dimension, quarter section of the directly loaded basket. The helium material is not shown.

The Rail-Pb system is also designed to maintain the temperature of critical components below their design limits during and after a 30 minute, fully engulfing, hypothetical accident condition (HAC) scenario. For fire accident scenarios lasting longer than the HAC fire described in 10 CFR 71.73, a significant amount of heat may be transferred to the interior of the cask. As in the Rail-Steel, the temperature of the neutron shield is expected to reach temperatures beyond the temperature limits. Heat then is dissipated by conduction through the gas layer in the neutron shield and by radiation between the outer wall of the intermediate shell layer and the outer enclosure shell. Similarly, the lead shell is expected to melt since its melting point is around 321°C (611°F). The impact limiters are made of wood encased in a thin metal layer and are

Deleted: fire accident

Deleted: longer period,

sealed to prevent moisture from deteriorating the wood over long periods of time. Since the impact limiters are assumed to stay intact (i.e., with the content sealed) after the initial accident event (e.g., derailment), the wood is not expected to char significantly. Charring is therefore not taken into account in this model.

IV.4.3 Rail-Pb Materials and Thermal Properties

The Rail-Pb is made of stainless steel, lead, copper, aluminum, NS-4-FR, Boral neutron absorber and helium. The inner and outer shell, the outer enclosure shell, the bottom plate, the vacuum flange, and the inner lid of the overpack are made from stainless steel, type 304. The gamma shield is made from copper-lead, and the outer lid from stainless steel, type 630. The radial channels are made from a combination of stainless steel, type 304, copper, and a small section of carbon steel. The stainless steel in the channel serves as the main support component while the copper enhances conduction through the channels. The overpack neutron shield is made from NS-4-FR. The impact limiters are redwood and balsa layers encased in a thin (stainless?) steel shell.

Comment [csb28]: Not familiar with this term.

In the fuel basket, the support disks, threaded rods, and spacer nuts are made from stainless steel, type 630, and the top and bottom support plates, short length cylinder, and fuel tubes from stainless steel, type 304. The heat transfer support disks are made from aluminum alloy 6061. As with the Rail-Steel, adjacent to each fuel tube wall is a layer of Boral sandwiched between the tube wall and a thin layer of stainless steel sheathing. The fuel rods are made from zircaloy or stainless steel cladding, but are assumed to be zircaloy as in the Rail-Steel analysis. The pellets are made from UO_2. The empty gas space, which encompasses most of the volume inside the overpack cavity, is filled with helium.

Deleted: $U0_2$

Tables IV-10 through IV-13 provide the thermal conductivity, specific heat, density, and emissivity for those materials used in the Rail-Pb which are different from the Rail-Steel, or for which the properties are significantly different (see Table IV-2 through Table IV-5 for additional properties). The properties of NS-4-FR reported in the Rail-Pb SAR are marginally different from those reported for Holtite-A, as expected. The thermal conductivity of redwood and balsa vary depending on the direction of the grain. For balsa, temperature dependent data is not found; therefore, values from MSC Patran material database are used and compared well with values in Incropera and Dewitt (1996). The MSC Patran database references are given in Tables IV-10. NUREG-0361 (1978) gives values through and along the grain for redwood; however, since the Rail-Pb SAR does not specifically describe the arrangement of the wood layers in the limiters, average properties (along and through the grain) are assumed. The specific heat and density of copper-lead provided in the Rail-Pb SAR are slightly lower and higher, respectively, than for plain lead (Incropera and Dewitt, 1996); properties from MSC Patran database are used instead since data is readily available above the melting temperature and included the specific latent heat of fusion (23.9kJ/kg [10.3Btu/lbm]). The specific heat of lead increases up to the melting point (by a factor of 1.07), but then remains approximately the same. Since these changes are small, the value at 92°C is used throughout the rest of the temperature range.

Comment [csb29]: What do the applicants use for this material property?

Table IV-10. Thermal conductivities for the Rail-Pb materials.

Material	Thermal Conductivity W/m-°C (Btu/ft-hr-°F)				
	92°C (200°F)	226°C (450°F)	377°C (700°F)	477°C (900°F)	726°C (1340°F)
Aluminum 6061[*]	171 (98.8)	176	176		
Copper[§]	402 (232.4)	386	376	369	352
Balsa[¥]	0.050	—	—	—	—
Lead[‡]	33.9 (19.6)	29.3 (16.9)	16.7 (9.7)	15.3 (8.8)	14.7 (8.5)
Redwood[€]	3.6 (2.0)	5.5 (3.1)	—	—	—
Stainless Steel Type	17.5 (9.9)	18.3 (10.6)	20.7 (12.0)	24.6 (14.2)	—

[*]Nuclear Acceptance Corporation International, 2004
[§]Incropera and Dewitt, 1996
[¥]McAdams, 1954; Perry, 1963; Weast, 1966
[‡]Kelley, 1960; Schorsch, 1966; Weast, 1966
[€]NUREG-0361, 1978

Table IV-11. Specific heat for the Rail-Pb materials.

Material	Specific Heat J/kg-K (Btu/lbm-F)				
	92°C (200°F)	226°C (450°F)	377°C (700°F)	477°C (900°F)	726°C (1340°F)
Copper[§]	390 (0.093)	406 (0.097)	422 (0.101)	431 (0.103)	451 (0.108)
Balsa[¥]	2302 (0.55)	—	—	—	—
Lead[‡]	131 (0.031)	—	—	—	—
Redwood[€]	2386 (0.57)	3898 (0.93)	—	—	—

Table IV-12. Densities for the Rail-Pb materials.

Material	Density kg/m^3 (lbm/ft^3)				
	92°C (200°F)	226°C (450°F)	377°C (700°F)	477°C (900°F)	726°C (1340°F)
Aluminum	2823 (176)	—	—	—	—
Copper[§]	8933 (558)	—	—	—	—
Balsa[¥]	130 (8.1)	—	—	—	—
Lead[‡]	11350 (709)	—	—	—	—
Redwood[€]	352 (22)	—	—	—	—

Table IV-13. Emissivity for some of the Rail-Pb materials.

Material	Emissivity
Aluminum 6061	0.22
Stainless Steel Type 630	0.58

With the exception of the basket and neutron region, all components are modeled explicitly. The impact limiters are modeled in their intact state, with properties of redwood and balsa since the outer shell volume is significantly smaller than the total wood volume. Contact gap effects are assumed negligible. As in the Rail-Steel model, NS-4-FR is replaced with air when the former reached its temperature limit, but only in the neutron shield region of the overpack. Radiation is activated in this region by setting the emissivity to the appropriate value.

IV.4.3.1 Directly Fuel Loaded Basket

In the Rail-Pb SAR, fuel rods are evaluated to determine a representative fuel rod configuration. The fuel assembly is then modeled explicitly to obtain an equivalent in-plane thermal conductivity for the homogenized fuel assembly, as described in Section IV.3.3.1. The fuel assembly axial conductivity is next obtained with an area weighted average using the thermal conductivities of the individual components of the fuel rods and helium. The directly loaded basket is then included explicitly in the normal condition run, but is not included in the subsequent regulatory fire accident run. Instead, the maximum temperature difference between the fuel basket and the inner wall of the overpack calculated in the normal condition run is added to the inner wall temperature of the overpack calculated in the regulatory fire run to obtain an estimate of the temperature of the center of the fuel basket for the regulatory run. A different approach is used for this study.

Deleted: here

The directly loaded fuel basket is replaced with a homogenized cylinder having equivalent effective thermal conductivities in the in-plane and axial directions. As described in Section IV.4.2, two variations of the same three-dimensional, quarter section, finite element model are generated. The first model included a support disk, a heat transfer disk, and the fuel tubes and helium space between the disks (see Figure IV-17). The second model did not include the heat transfer disk; instead, it is replaced with helium and the boundary conditions are modified to reflect this change.

The in-plane and axial thermal conductivities of the fuel basket are replaced with an equivalent thermal conductivity using the following four step procedure borrowed from the Rail-Steel SAR and modified here to address this particular model. First, the detail cross section of the fuel assembly is replaced with a homogenized fuel region having equivalent thermal properties. This analysis is done in the Rail-Pb SAR, as explained above, and the analysis results are included in this study. As expected, the thermal conductivity reported in the Rail-Pb SAR are close to those reported in Rail-Steel SAR for similar fuel assemblies, which serves as a check. Second, the fuel

Deleted: y

Deleted: ies

Deleted: ough

Comment [csb30]: By using a method of analysis from one vendor to evaluate a package from another vendor, are we tacitly approving or endorsing the

Deleted: d

tube, Boral, and stainless steel sheathing are replaced with a homogenized wall having an equivalent thermal conductivity as described in the Rail-Pb SAR.

Third, the two, three-dimensional, quarter section models described above are used to obtain the in-plane and axial effective thermal conductivities. Both these models are evaluated with two sets of boundary conditions:

(1) a uniform circumferential temperature applied across the circumferential wall of the model; adiabatic conditions over the axial ends; and uniform heat generation in the homogenized fuel assemblies; and

(2) a uniform temperature over one axial end; a uniform heat flux over the other axial end; and adiabatic conditions over the circumference.

Comment [csb31]: Not clear as to exactly what is being done here.

In the first case, the in-plane thermal conductivity is obtained using the same procedure described in Section IV.3.3.1. In the second case, the axial thermal conductivity is obtained using the standard relationship:

$$k_{eff} = \frac{qA}{L(T_q - T_t)}$$

Here A is the cross sectional area of the basket; L is the thickness across the modeled section; q is the uniform heat flux applied over one of the cross sectional area, axial ends; and T_t is the uniform temperature applied over the other cross sectional area, axial end. T_q is the average temperature where uniform heat flux is applied and is calculated using the simulation results. A second option is to apply constant temperatures at both axial ends of the basket, then calculate the total heat flow (qA) through the basket using the simulation results, and lastly calculate the effective axial conductivity using the above equation. To obtain temperature dependent thermal conductivities, this third step is repeated a number of times using a wide range of uniform circumferential temperatures and applied heat fluxes.

Fourth, the thermal conductivities obtained in the previous step are added using an equivalent thermal resistor network model to obtain in-plane and axial thermal conductivities, respectively, over the entire fuel basket.

Table IV-14 shows the thermal properties used for the basket. These properties are applied to the homogenized fuel-basket cylinder. The equivalent specific heat and density are obtained using a mass and volume weighted average, respectively, over the individual component properties. The volume of each component in the fuel basket (i.e., support disks, heat transfer disks, fuel tubes, etc.) is given in the Rail-Pb SAR.

Table IV-14. Effective thermal properties of the directly loaded fuel basket.

Effective Thermal Properties	92°C (200°F)	226°C (450°F)	377°C (700°F)	477°C (900°F)	726°C (1340°F)
Radial Thermal	3.2 (1.8)	3.8 (2.1)	4.3 (2.4)	5.0 (2.8)	5.9 (3.4)
Axial Thermal Conductivity	2.4 (1.4)	3.2 (1.8)	3.8 (2.1)	4.5 (2.6)	5.8 (3.3)
Specific Heat	332 (0.079)				
Density	2450 (153)				

IV.4.3.2 Neutron Shield Region

The neutron shield region is modeled using the same approach used in the SARs (Nuclear Assurance Corporation International, 2004, Holtec International, 2004). Both reports used the thermal resistor network method to obtain the in-plane and axial effective thermal conductivities (see Section IV.3.3.4). In the case of the Rail-Pb, there are fewer radial channels than in the Rail-Steel; however, as will be demonstrated shortly, this shortcoming is compensated for by adding copper in the neutron shield region. Table IV-15 shows the thermal properties used for the neutron shield region in the Rail-Pb. The circumferential thermal conductivity is assumed to be that of NS-4-FR. As before, the specific heat and density are obtained from a mass and area weighted average. Note the thermal conductivity is slightly higher than in the Rail-Steel even though the Rail-Pb contains fewer channels. This is expected since the neutron shield in the Rail-Pb contains copper which has a much higher thermal conductivity than carbon steel.

Deleted: Acceptance

IV.4.4 Rail-Pb P-Thermal Finite Element Model

The following description is short since most of the details are similar to the Rail-Steel analysis described in Section IV.3.4. In the Rail-Pb runs, the cask model had 109662 elements (see Figure IV-18); this corresponds to a nominal element size of 10.2cm (4in). The element count is less than in the Rail-Steel since the Rail-Pb is smaller and has fewer features which add to the element count. A mesh refinement study is also conducted with the Rail-Pb model with a similar outcome. The boundary conditions for the normal condition, steady-state run, the regulatory uniform heating run, and the CAFE fire runs are the same as discussed in Sections IV.2 and IV.3.4. They are not repeated here.

IV.4.5 Rail-Pb Thermal Analysis Results

The following figures (see pages 54 through 62) show additional results for the Rail-Pb not provided in Chapter 4. Figure IV-19 shows results for the regulatory uniform heating case. Recall this is a P-Thermal only run. Figure IV-20 shows results for the regulatory CAFE fire; Figure IV-21 shows results for the fully engulfing CAFE fire run with the cask on the ground; and Figures IV-22 and IV-23 show results for the CAFE fire runs with the cask on the ground and outside the pool area. As with the Rail-Steel, the last three cases are run for a total of three hours. A discussion of these results and their implications is provided in Chapter 4.

Table IV-15. Effective thermal conductivities for the neutron shield region of the Rail-Pb.

Effective Thermal Properties	92°C (200°F)	226°C (450°F)	377°C (700°F)	477°C (900°F)	726°C (1340°F)
In-Plane Thermal Conductivity W/m-°C	8.1 (4.6)	7.9 (4.5)	7.7 (4.4)	7.7 (4.4)	7.4 (4.2)
Axial Thermal Conductivity W/m-°C (Btu/ft-hr-°F)	7.6 (4.3)	7.3 (4.2)	7.3 (4.2)	7.2 (4.1)	6.9 (3.9)
Specific Heat J/kg-°C (Btu/lbm-°F)	1406 (0.33)	535 (0.12)	563 (0.13)	575 (0.13)	611 (0.14)
Density kg/m^3 (lbm/ft^3)	1983	380 (23)			

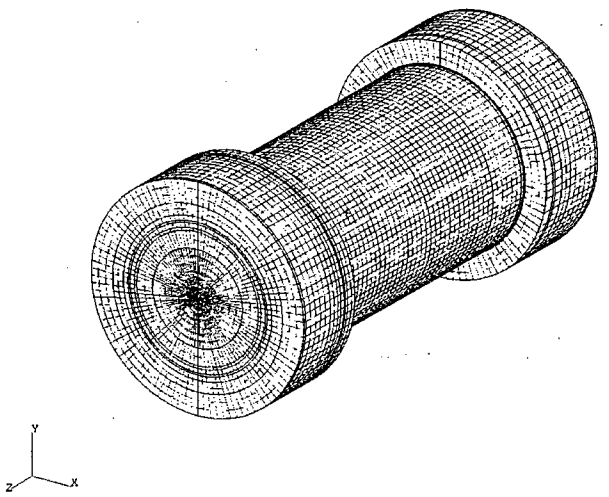

Figure IV-18. The Rail-Pb mesh.

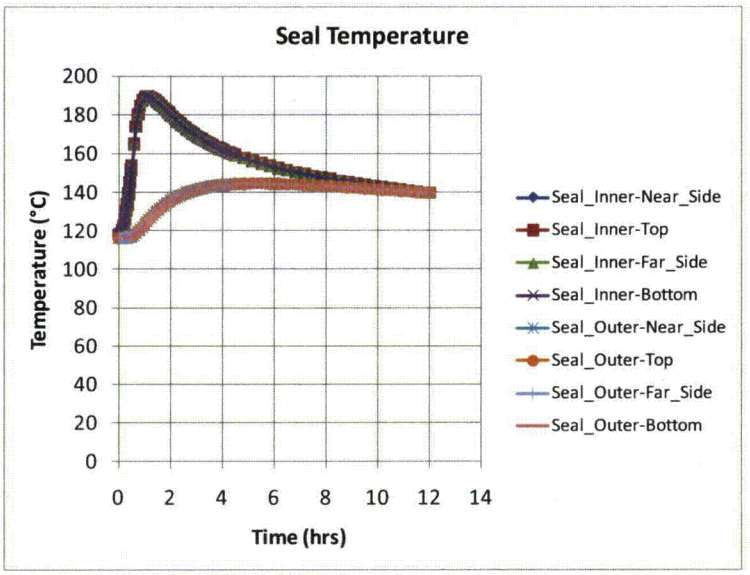

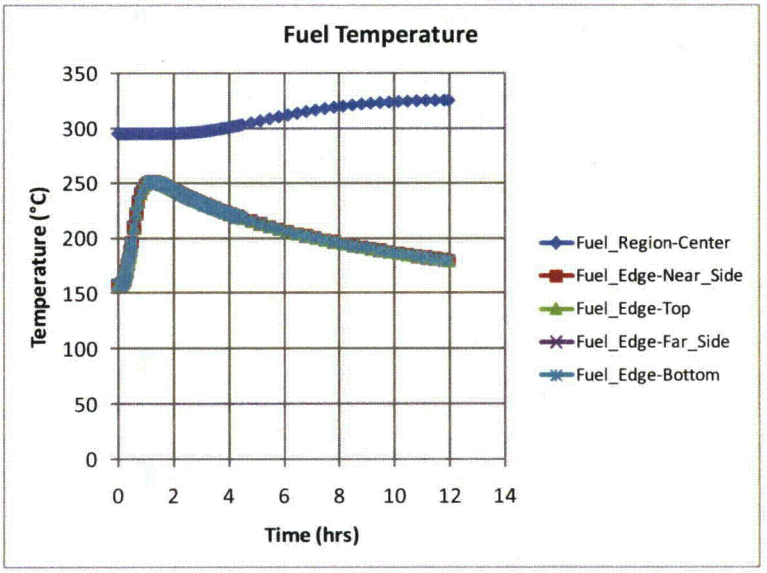

Figure IV-19. Rail-Pb Regulatory Uniform Heating Results

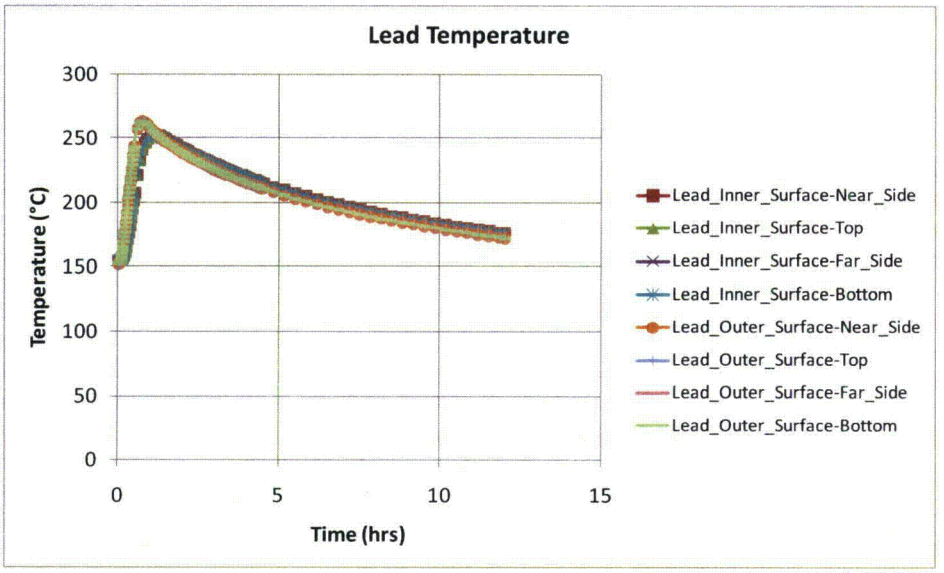

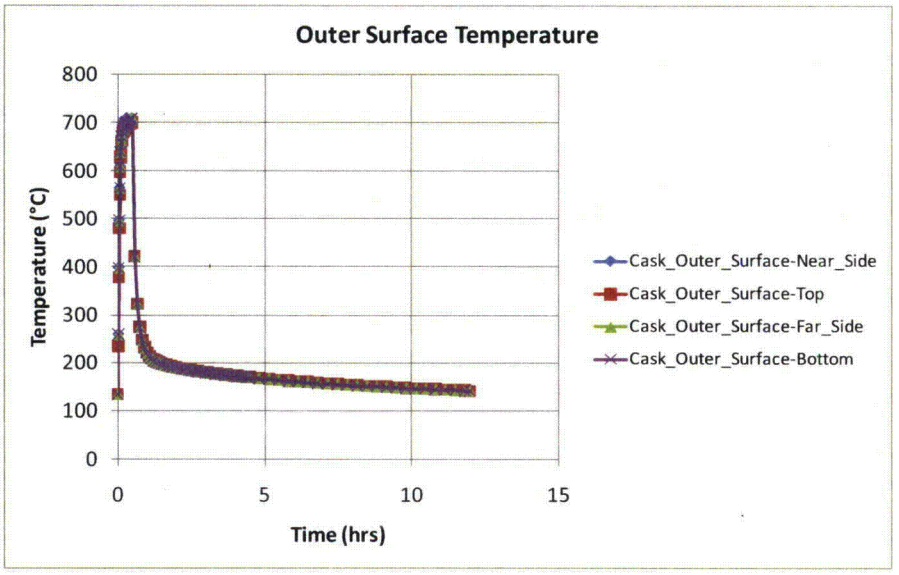

Figure IV-19. Rail-Pb Regulatory Uniform Heating Results - Continue

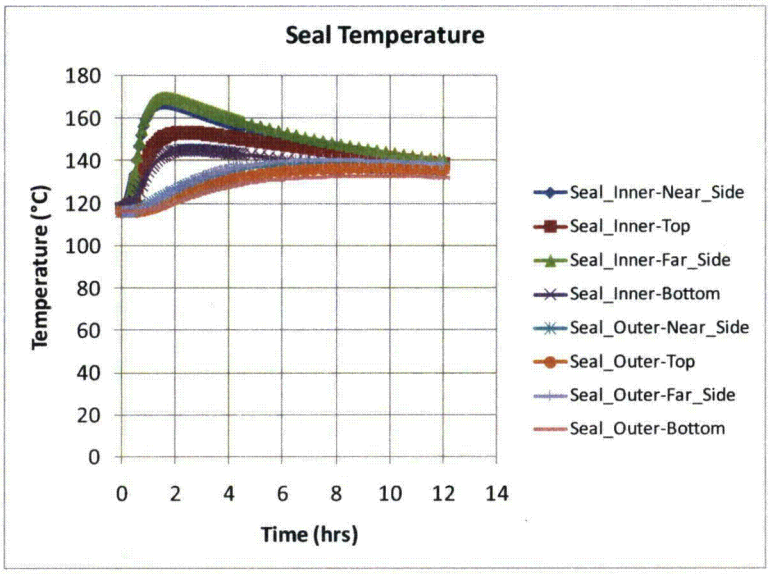

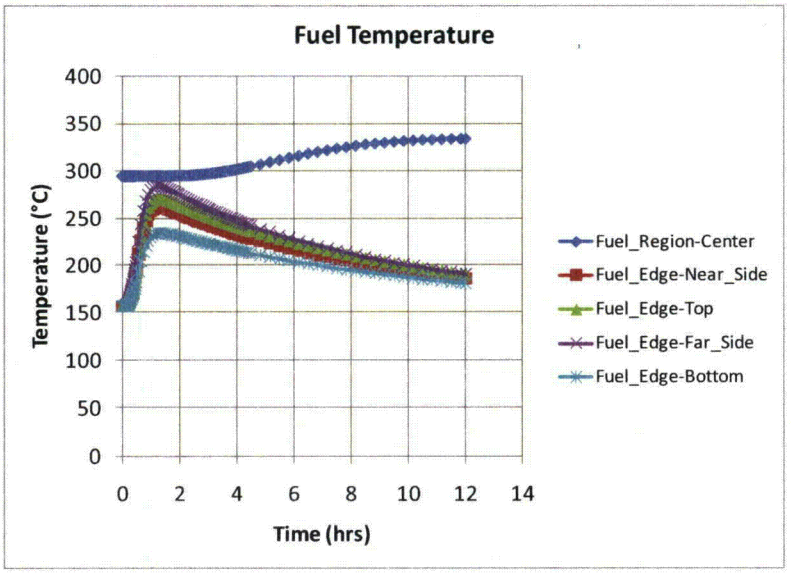

Figure IV-20. Rail-Pb CAFE Regulatory Fire

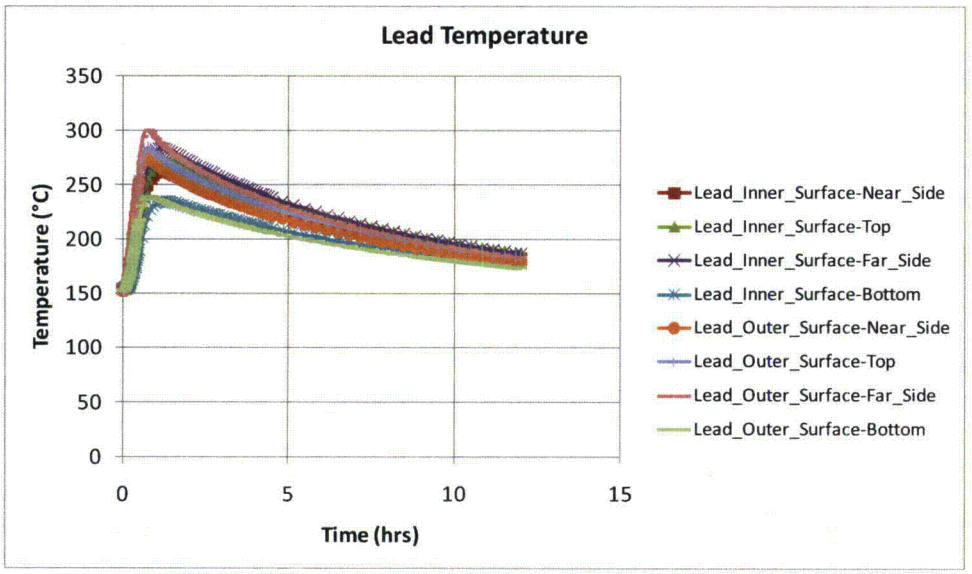

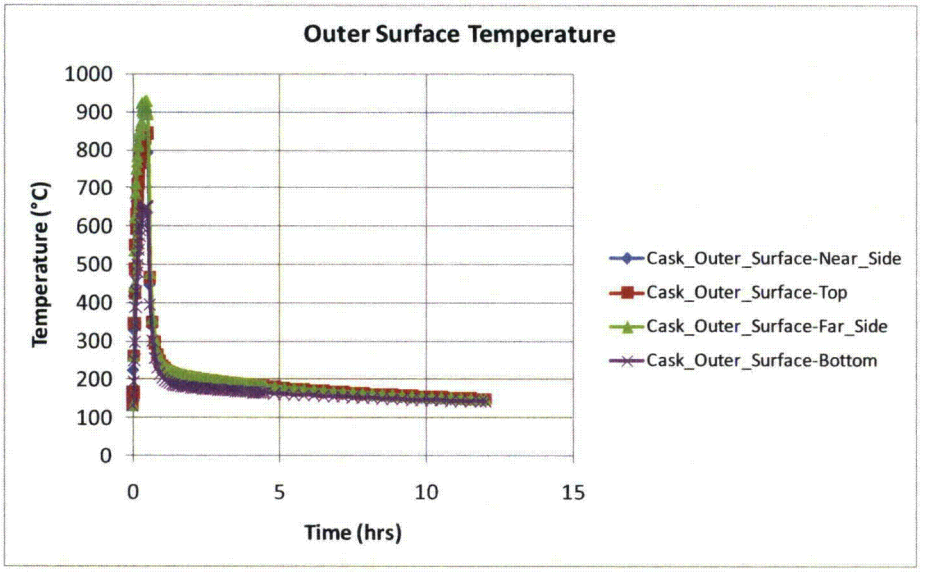

Figure IV-20. Rail-Pb CAFE Regulatory Fire - Continue

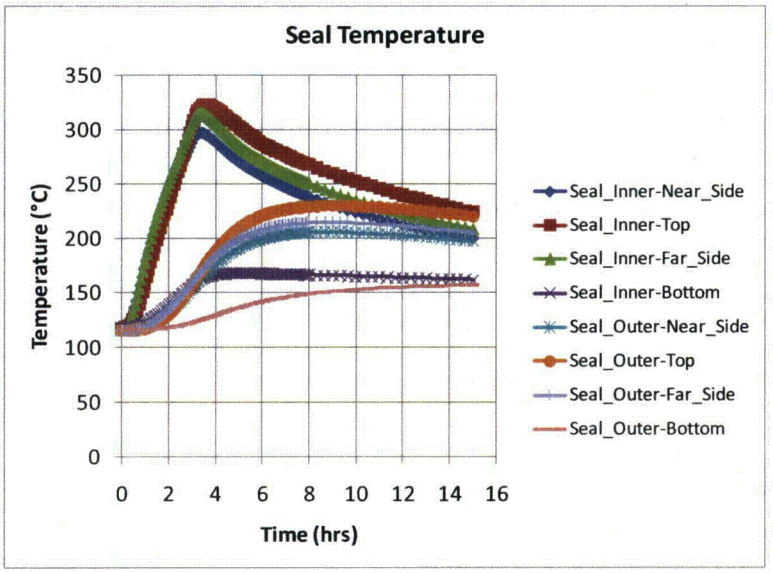

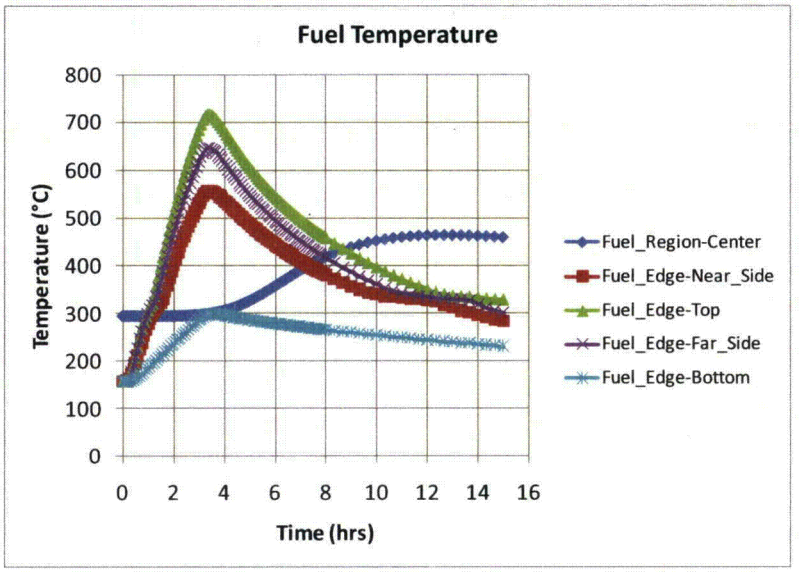

Figure IV-21. Rail-Pb cask on ground at the pool center.

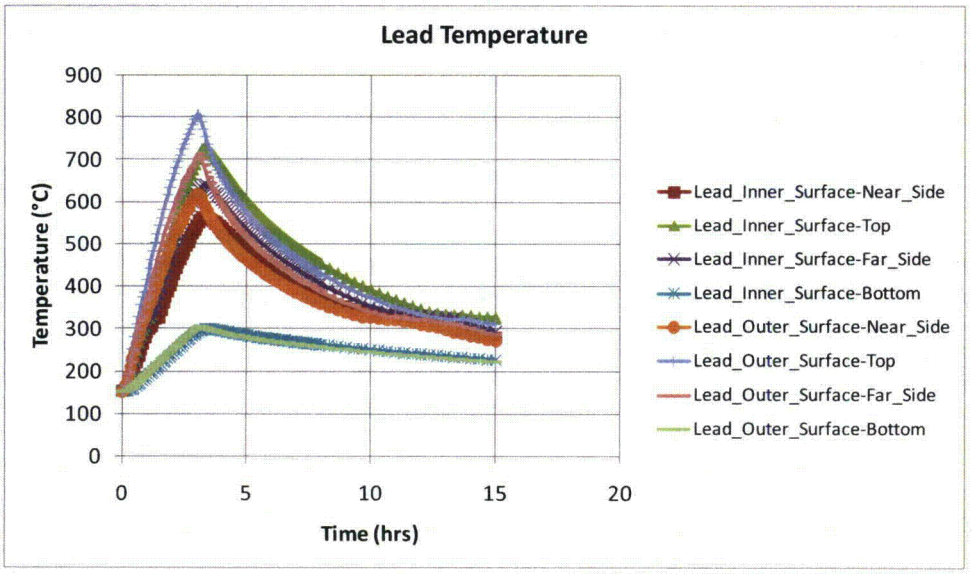

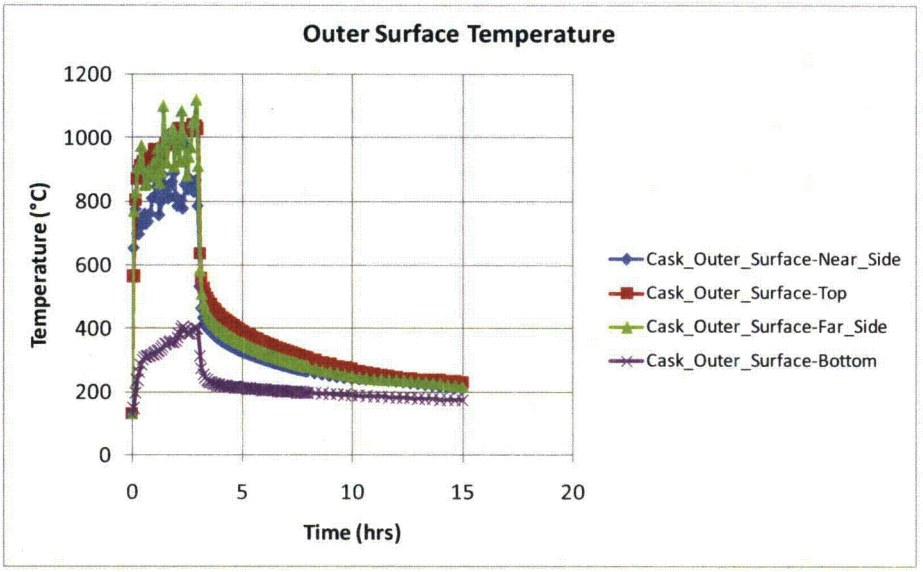

Figure IV-21. Rail-Pb cask on ground at the pool center. - Continue

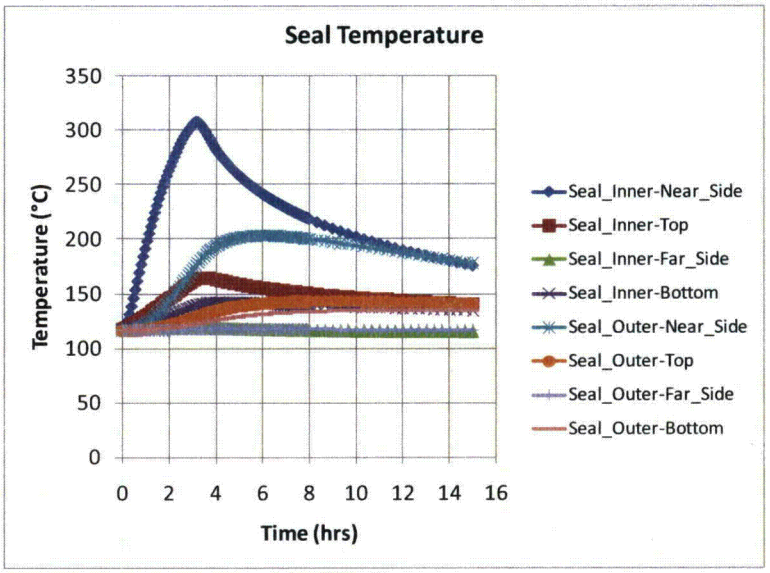

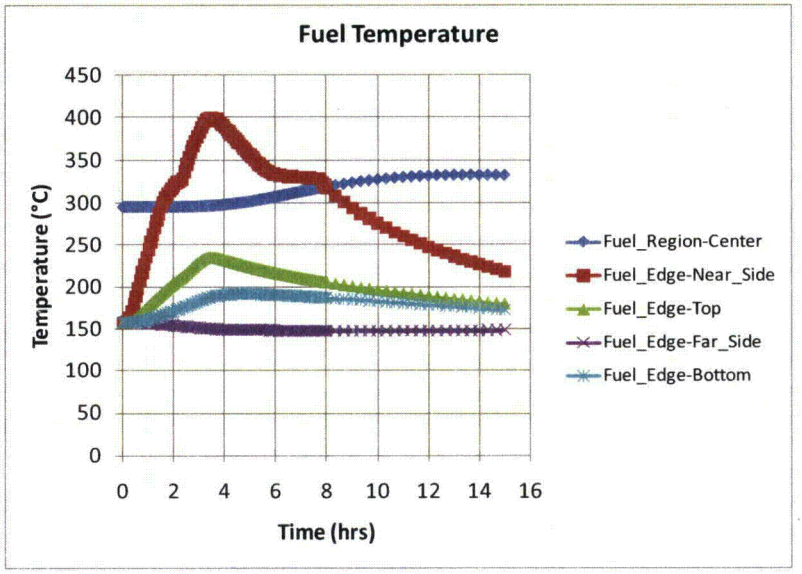

Figure IV-22. Rail-Pb cask on ground 3.0m (10ft) from the edge of the pool.

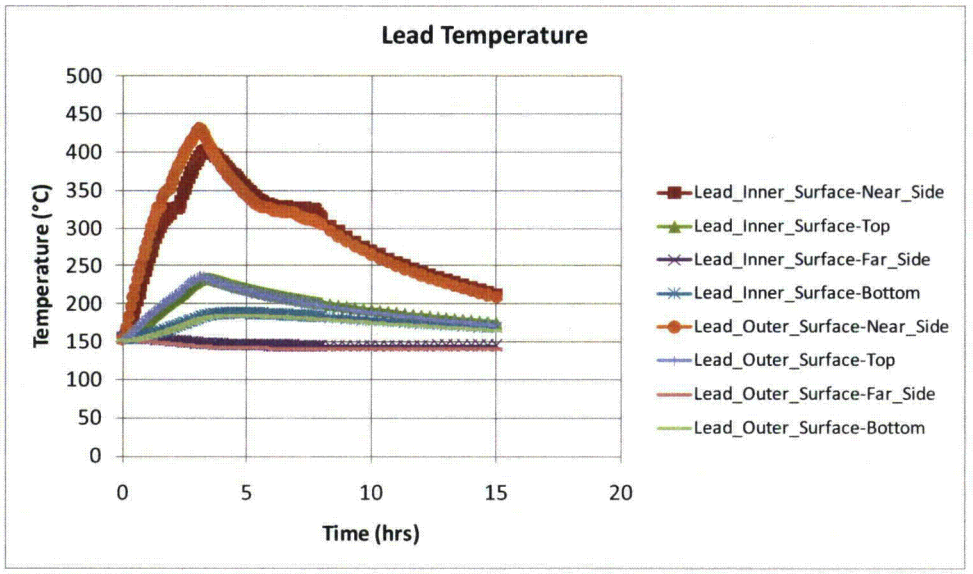

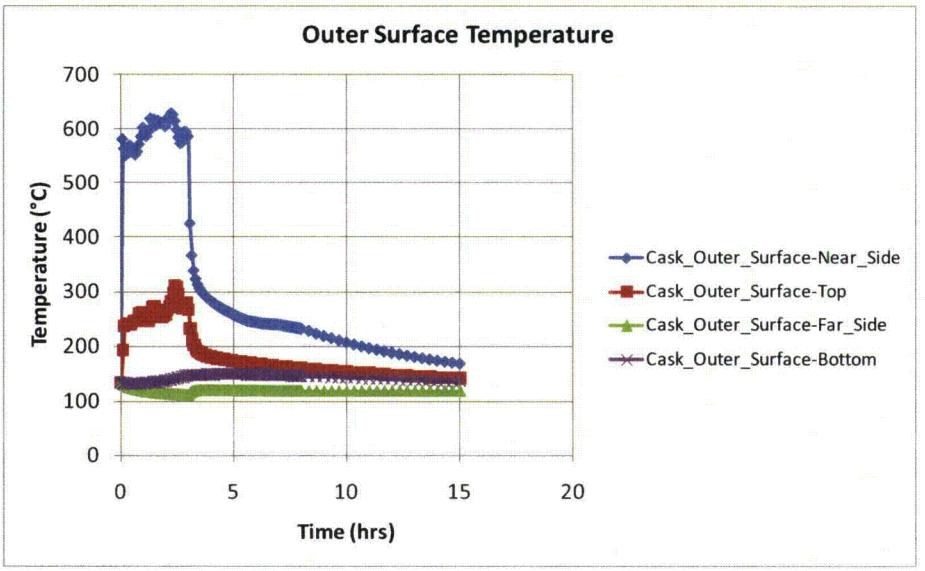

Figure IV-22. Rail-Pb cask on ground 3.0m (10ft) from the edge of the pool. - Continue

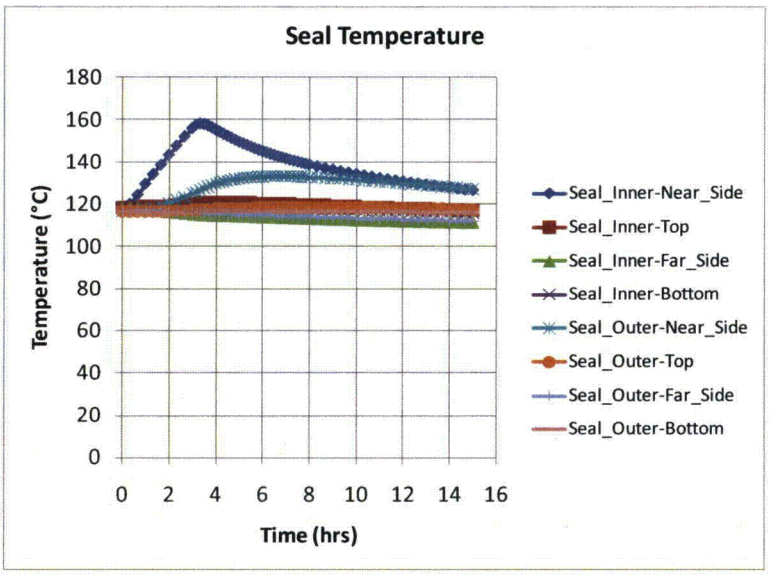

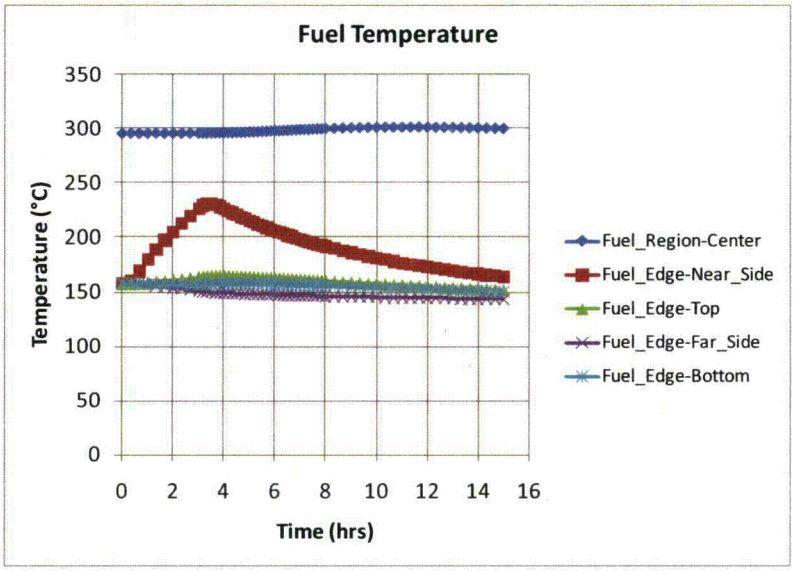

Figure IV-23. Rail-Pb cask on ground 18.3m (60ft) from the edge of the pool.

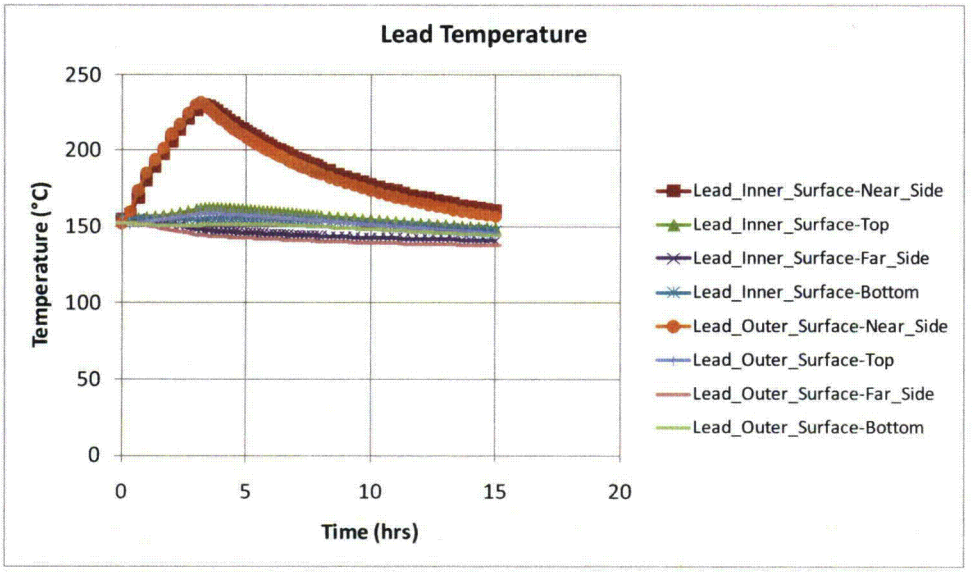

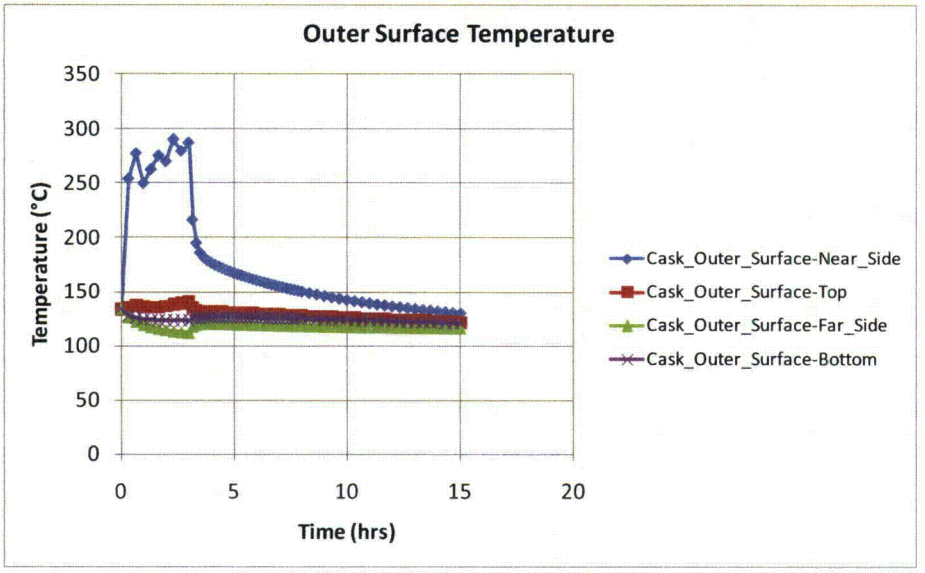

Figure IV-23. Rail-Pb cask on ground 18.3m (60ft) from the edge of the pool. - Continue

IV.5 CAFE Benchmark

Large, fully-engulfed objects have a great impact on the surrounding fire environment. To adequately predict incident heat flux to casks, computational fluid dynamics models must be employed with appropriate boundary conditions. Also, because of the impact that massive objects have on fires, computational fluid dynamics models must be validated against experimental data from tests that have similar size objects (Nicolette and Larson, 1989).

Since the development of the CAFE code (del Valle, et. al., 2009; del Valle, 2007; Are et.al., 2005; Lopez et. al., 2003), there has been a continuing effort to benchmark and fine-tune this fire model by making use of relevant empirical data from experiments. Continuing with this effort, prior to running the cases described in Chapter 4, CAFE is benchmarked against experimental data obtained from two fire test series conducted at Sandia National Laboratory Lurance Canyon Burn Site: (1) one using a large calorimeter in the center of the pool (Greiner, 2009; Kramer, 2008), and (2) the other using a smaller diameter calorimeter adjacent to the fire (Lopez et. al., 2003). The large calorimeter is close to the size of the casks analyzed in this study, and had a test setup and conditions that closely matched the regulatory hypothetical fire accident scenario outlined in 10CFR71.73 for certification of SNF transportation packages. The smaller diameter calorimeter test is used to benchmark CAFE's ability to predict heat flux to objects outside the fire plume. This section briefly describes these experiments, and shows benchmark results.

Deleted: nuclear spent fuel

IV.5.1.1 Large Calorimeter Test and Benchmark Results

The large calorimeter is a carbon steel cylindrical pipe approximately 2.43m (96in) in diameter and 4.6m (180in) in length, with nominal 2.54cm (1in) thick walls, and had bolted lids on each end (see Figure IV-24a). The calorimeter is placed on two stands at the center of a 7.93m (26ft) diameter fuel pool. The stands maintained the calorimeter 1m (39.4in) above the fuel surface. Approximately 2000 gallons of JP8 are used per test. Total burn time vary with tests, but is at least 25 minutes. All tests are conducted in relatively low wind conditions (<5m/s) to assure the calorimeter is fully or partially engulfed (see Figure IV-24b.)

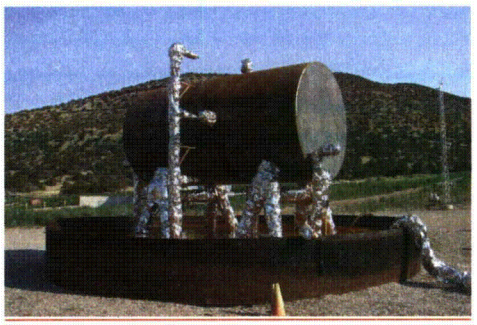

(a) (b)

Figure IV-24. Large calorimeter fire test: (a) test setup and (b) fire fully engulfing the calorimeter.

Thermocouples are installed on the interior walls of the calorimeter to measure interior surface temperatures. All TCs are installed in a ring configuration as shown in Figure IV-25. Heat flux gages are placed just outside the round walls of the calorimeter in a ring configuration and outside the lids to measure incident heat fluxes close to the outer walls of the calorimeter. Fuel burn rates are measured using a TC rake. Directional flow probes are installed just outside of the calorimeter walls to measure the flow speed of hot gases near the calorimeter walls. Finally, ultrasonic sensors placed on four towers—two sensor towers aligned with the calorimeter lids and two sensor towers perpendicular to the cylindrical section of the calorimeter, but on opposite sides—are used to measure wind speed and wind direction. Each tower is approximately 24.4m (80ft) from the center of the pool and had three ultrasonic sensors 2, 8 and 10m (6.5, 26.2, and 32.8ft) from the ground.

Comment [csb32]: May not be clear on what this is.

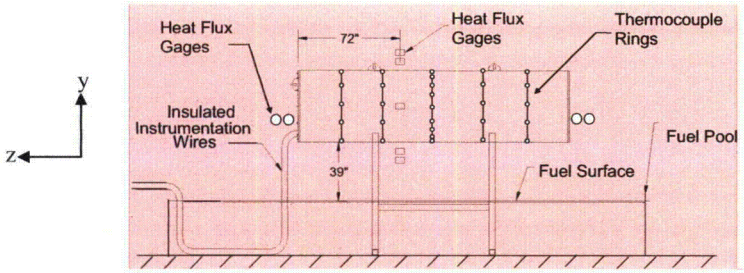

Figure IV-25. Side view (looking from the north) of calorimeter and test setup. Note: the calorimeter is centered with the pool. This drawing is not to scale.

Comment [csb33]: This figure did not come out when I printed the document.

Figure IV-26a shows average temperatures along the four circumferential sides of the calorimeter obtained from Test 1 and from the CAFE benchmark run. Data from Test 1 is chosen because the wind conditions and fire characteristics of this test best matched the regulatory conditions specified in 10CFR71.73 and the fire scenarios analyzed in this study. The test readings are taken from thermocouples located at 0 (north side, i.e., pointing out of the page), 90 (top side), 180 (south side, i.e., pointing into the page) and 270 (underneath) degrees. This plot illustrates that average temperature predictions obtained from CAFE envelope the average temperatures readings from the test.

Deleted: From this perspective, however, CAFE over predicts temperatures underneath and on the south side of the calorimeter, and under predicts temperatures on the top of the calorimeter. Figure IV-26b shows a plot of average temperatures over each thermocouple ring starting from the left side of the calorimeter and moving along the negative z-axis as shown in Figure IV-25. From this perspective CAFE predicts the average temperatures over the rings reasonably well.

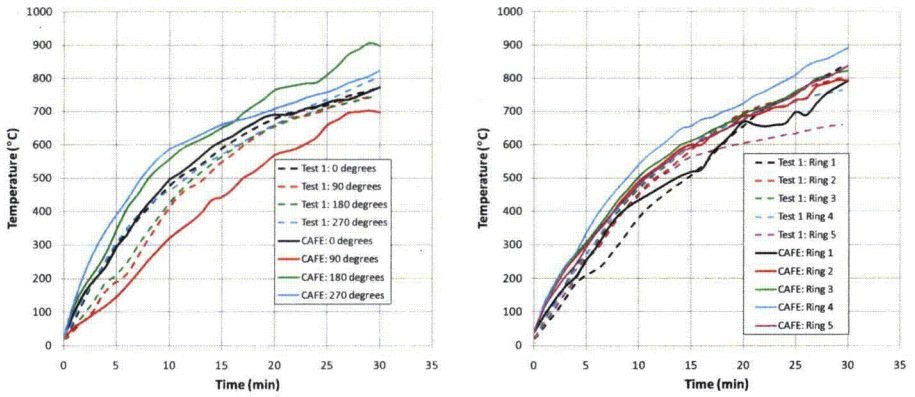

(a) (b)

Figure IV-26. CAFE benchmark results using fully engulfed large calorimeter: (a) temperatures average along the 0, 90, 180, and 270 degree side looking at the calorimeter from the negative z-direction, and (b) temperatures averaged over each ring starting from Ring 1 located on the positive side of the z-axis.

From this perspective, however, CAFE over predicts temperatures underneath and on the south side of the calorimeter, and under predicts temperatures on the top of the calorimeter. Figure IV-26b shows a plot of average temperatures over each thermocouple ring starting from the left side of the calorimeter and moving along the negative z-axis as shown in Figure IV-25. From this perspective CAFE predicts the average temperatures over the rings reasonably well.

Formatted: Space After: 6 pt

Closer inspection of the temperatures histories obtained from CAFE at each of the nodes corresponding to thermocouple locations revealed excellent agreement with test data over most of the cask, except at locations are the wind effects are strongest, the last two rings to the right of Figure IV-25 at 90 (top side), 180 (south side) and 270 (underneath) degrees. Temperatures at 180 and 270 degrees are higher than expected, while temperatures at 180 degrees are under predicted. Differences rapidly diminished going from the rings on the right side of the calorimeter to the rings on the left side as shown in Figure IV-25. Part of the reason for these discrepancies is the way in which the wind boundary conditions are applied in the computational fluid dynamics model. In the large calorimeter test series, wind speeds are obtained only at four locations around the pool, and at three heights. These height dependent data are applied uniformly over the corresponding cross sections of the domain, which does not necessarily reflect the actual conditions in the test. This leads to wind speeds being higher than expected in some locations around the casks such as the south side of the cask near the ring 5 (rightmost ring in Figure IV-25).

Deleted: ¶

IV.5.1.2 Small Calorimeter Test and Benchmark Results

Experimental data form a smaller pipe calorimeter is used to benchmark the view factor method used in CAFE (Lopez et al., 2003). The CAFE model for thermal radiation transport within and

near large hydrocarbon fires is divided into two types, diffusive radiation inside the flame zone and clear air or view factor radiation outside the flame zone. Outside the flame zone, thermal radiation transport is modeled by the clear air or view factor method. The calculation of the view factor between the fire and an adjacent object is complicated due to the fact that the outer surface of a fire (or smoky region) is dynamically changing due to the puffing and turbulent nature of flames (Lopez et. al., 2003).

In the experiments, a calorimeter is positioned such that its axis is 1.5m (4.9ft) away from the center of the fuel pool. The wind blew the fire away from the calorimeter leaving a significantly larger gap between the pipe calorimeter and the plume. Results from tests and CAFE are presented in Figure IV-27. The temperatures shown are at the center ring of this calorimeter. The blue lines are obtained from experimental data and the black lines are obtained from CAFE. By looking at the temperature distribution of this very long pipe, it can be clearly seen how the external radiation algorithm worked on the far field object.

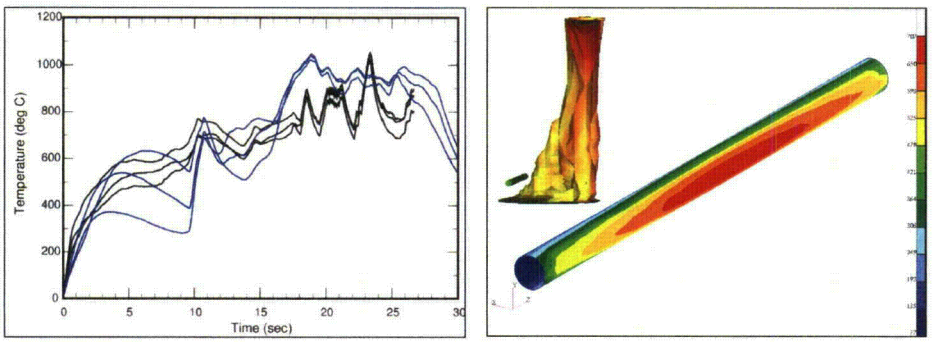

Figure IV-27. CAFE benchmark results using a small calorimeter 1.5m (4.9ft) from the edge of the fire.

Some kind of summary or conclusion of the CAFÉ testing?

How about an overall summary or conclusion for this Appendix?

Formatted: Left